

Spin-polarized ^3He - ^4He solutions: Longitudinal spin diffusion and nonlinear spin dynamics

G. Nunes, Jr.,* C. Jin, D. L. Hawthorne, A. M. Putnam, and D. M. Lee

Laboratory of Atomic and Solid State Physics, Cornell University, Ithaca, New York 14853

(Received 18 March 1992)

Pulsed-NMR techniques have been used to investigate longitudinal spin diffusion and nonlinear spin dynamics in dilute, spin-polarized ^3He - ^4He solutions between 4 and 400 mK. Solutions with ^3He concentrations $x_3 = 3.5 \times 10^{-4}$ and 19.4×10^{-4} were forcibly polarized to as much as 65% and 25%, respectively, with a 9.2-T magnetic field. A technique for measuring the coefficient of longitudinal spin diffusion D_{\parallel} is described, and the results of the technique are compared with recent theoretical calculations. Throughout a temperature range that covers both degenerate and nondegenerate behaviors, theory and experiment are found to be in excellent quantitative agreement for $x_3 = 3.5 \times 10^{-4}$, and in somewhat weaker agreement for $x_3 = 19.4 \times 10^{-4}$. The presence of strong molecular fields in this system is confirmed by the observation of multiple spin echoes, but it is found that they are not adequately described by recent theory. In addition, the observation of a novel, extremely long-lived oscillation with a lifetime on the order of 10 sec is reported. These oscillations are found to have sensitive temperature and magnetic-field-gradient dependencies. A simple model which implies that this behavior is driven by a nonlinear instability is presented, and the results of numerical simulations based on this model are examined in an attempt to gain further insight into the spin dynamics of the system.

I. INTRODUCTION

The spin dynamics and transport properties of spin-polarized Fermi systems have been the subject of much recent experimental and theoretical interest.¹ Dilute solutions of ^3He in superfluid ^4He provide a nearly ideal system in which to carry out studies of such phenomena. They can be highly polarized at readily attainable magnetic fields and temperatures, and can be examined both in the degenerate ($T \ll T_F$) and classical, or Boltzmann, ($T \gg T_F$) regimes. They remain the only Fermi system that can be studied in the transition region *between* degenerate and classical behaviors. At the low concentrations of interest, the ^3He atoms are weakly interacting, and so form a quantum gas, rather than a strongly interacting liquid. This last point is particularly important from a theoretical point of view, as it greatly simplifies any calculation of the transport coefficients in the system.

Nonlinear spin diffusion in degenerate Fermi systems was examined by Leggett and Rice,^{2,3} who showed that quantum exchange effects in pure (normal) ^3He give rise to a molecular field whose strength depends both on the degree of polarization, and on the details of the ^3He - ^3He interactions. This molecular field cannot directly affect the precession of the local polarization $\mathbf{M}(\vec{r}, t)$, since the two are constrained to be parallel. (In this paper we shall use boldface type to denote vectors in spin space. Real-space vectors, gradients, etc., will be denoted by arrows, or will have their Cartesian components written out explicitly.) The molecular field can, however, affect the spin *currents*, which then react back on \mathbf{M} through the continuity equation. The relative importance of these ex-

change effects depends on the ratio of the spin-diffusion relaxation time τ_D to the time it takes a quasiparticle to execute a single precession (at frequency Ω_{int}) about the local molecular field. Following Leggett,³ we can characterize the strength of this molecular field by the quantity $\mu M \equiv \Omega_{\text{int}} \tau_D$, where $M = |\mathbf{M}|$ is the degree of polarization, and μ is the dimensionless "spin rotation" parameter. If $\mu M \gg 1$, then a quasiparticle will execute many cycles about the local molecular field before being relaxed in a collision, and the exchange effects will be important. Leggett's predictions³ for the behavior of a ϕ -180° spin-echo experiment under these circumstances have been experimentally verified by Corruccini *et al.*⁴ for both pure ^3He and concentrated ^3He - ^4He mixtures.

More recently, Bashkin has argued that quantum exchange should lead to similar molecular-field effects in polarized systems which are at low temperatures, but still obey Boltzmann statistics, rather than degenerate quantum statistics.⁵ In these systems, the thermal de Broglie wavelength Λ_T becomes much longer than the range of the interparticle potential (which at low temperatures we may take to be the *s*-wave scattering length a), so that quantum-mechanical corrections to the scattering become important. In an independent treatment, Lhuillier and Laloë⁶ examined the effect of these quantum corrections in detail, and found that forward scattering exchange gives rise to an additional precession of the particle spins, which they termed "the identical spin rotation effect." Since this additional precession has the same effect on the spin dynamics as the molecular field in the degenerate Fermi liquid, it is entirely reasonable to find that Lhuillier and Laloë's nonlinear spin-diffusion

equation for dilute gases is identical to that originally given by Leggett.³

The similarity of the spin dynamics in the low-density, weakly interacting gas to those in the high-density, strongly interacting liquid suggests that a more unified approach ought to be possible. Such a unified approach has, in fact, been carried out by Lévy and Ruckenstein,⁷ who developed a quasiparticle description of paramagnetic Boltzmann gases that emphasizes their relation to more dense systems. They have successfully applied that approach to the results of experiments on spin-polarized atomic hydrogen gas.⁸

In both the degenerate and Boltzmann regimes, the essential effect of the molecular field on the spin dynamics can be seen from Leggett's equation for the steady-state spin currents in the Larmor (rotating) frame,

$$\vec{J} = -D_s \vec{\nabla} \mathbf{M} - \vec{J} \times \mu \mathbf{M}, \quad (1.1)$$

where D_s is the coefficient of spin diffusion, $\vec{\nabla}$ is the real-space gradient operator, and the spin current \vec{J} has both spin and spatial vector components. From the second term on the right-hand side, it is apparent that, in addition to being driven by gradients in \mathbf{M} , the spin currents precess about the local molecular field $\mu \mathbf{M}$. The solution to this equation is easily found to be³

$$\vec{J}(\vec{r}, t) = -\frac{D_s}{1 + \mu^2 M^2} [\vec{\nabla} \mathbf{M} + \mu(\mathbf{M} \times \vec{\nabla} \mathbf{M}) + \mu^2(\mathbf{M} \cdot \vec{\nabla} \mathbf{M})\mathbf{M}], \quad (1.2)$$

which, together with the continuity equation for the polarization (again, in the rotating frame)

$$\frac{\partial \mathbf{M}}{\partial t}(\vec{r}, t) + \vec{\nabla} \cdot \vec{J}(\vec{r}, t) - \mathbf{M} \times \gamma \delta \mathbf{H}(\vec{r}) = 0, \quad (1.3)$$

completely defines the spin dynamics of the system. $\delta \mathbf{H}(\vec{r})$ is the residual (gradient) part of the applied field that is not removed by transforming to the rotating frame, and γ is the ^3He gyromagnetic ratio.

Given the complex form of these equations, it is not surprising that spin-polarized gases and liquids exhibit a rich variety of nonlinear phenomena. In addition to the spin-echo behavior verified by Corruccini *et al.*,⁴ Eqs. (1.2) and (1.3) predict multiple spin echoes,⁹ as well as spin waves. The latter have been observed in pure ^3He ,¹⁰ in concentrated (degenerate) ^3He - ^4He solutions,¹¹⁻¹³ as well as in spin-polarized atomic hydrogen⁸ and ^3He (Ref. 14) gases. More recently, Candela *et al.* have observed spin waves in dilute ^3He - ^4He solutions that are in the intermediate regime between the degenerate and classical limits.¹⁵ The earliest investigation of such a highly polarized, intermediate regime ^3He - ^4He solution, however, was undertaken by Gully and Mullin,¹⁶ who carried out a Leggett-Rice-type ϕ - 180° spin-echo experiment, which they analyzed to obtain both μM and D_s . At high temperatures, where the solution obeyed classical statistics, their measured values for these two quantities agreed well with theoretical predictions, and confirmed the presence of identical spin rotation effects in spin-polarized dilute solutions. At lower temperatures, where the system should cross over to degenerate behavior, however, they

found that μM , instead of increasing more sharply with decreasing T , leveled off and even decreased at the lowest temperature. They also found that D_s , instead of making a smooth transition between an approximately \sqrt{T} behavior at high temperatures and a $1/T^2$ dependence in the degenerate regime, began to fall quite sharply with decreasing temperature just at the point it might have been expected to level off or even increase.

A possible explanation for the unexpected behavior of both D_s and μM was put forward by Meyerovich,¹⁷ who argued that in a system that was both degenerate and spin polarized, the spin currents perpendicular (in spin space) to the direction of polarization should relax on a time scale τ_\perp significantly shorter than the relaxation time τ_\parallel for the parallel spin currents. As a result, the system should no longer have a single spin-diffusion coefficient, but rather two: D_\perp for the relaxation of the transverse spin currents, and D_\parallel for the relaxation of the longitudinal spin currents. Since a ϕ - 180° type spin-echo experiment will only be sensitive to D_\perp , any interpretation of such an experiment based only on Leggett's original analysis may well encounter difficulties.

While the argument for anisotropic spin diffusion can be made on general grounds,^{17,18} Jeon and Mullin¹⁹ have shown that a more detailed treatment of the kinetics also gives two relaxation times, with $\tau_\perp \ll \tau_\parallel$ for small T/T_F and large M . They find that, under these conditions, Leggett's equation for the spin currents should be somewhat modified. If the spin-space unit vector $\hat{\ell}$ is defined such that $\mathbf{M} = M\hat{\ell}$, then Eq. (1.2) decouples into separate expressions for the longitudinal ($\vec{J} \parallel \hat{\ell}$) and transverse ($\vec{J} \perp \hat{\ell}$) spin currents. In the degenerate, spin-polarized regime, Jeon and Mullin find

$$\vec{J}_\parallel = -D_\parallel \vec{\nabla} M \hat{\ell} \quad (1.4)$$

and

$$\vec{J}_\perp = -\frac{D_\perp}{1 + \mu^2 M^2} [M \vec{\nabla} \hat{\ell} + \mu M^2 (\hat{\ell} \times \vec{\nabla} \hat{\ell})], \quad (1.5)$$

with (for example) $D_\perp \sim \frac{1}{2} D_\parallel$ at $T/T_F = 0.1$ if the system is 60% polarized.¹⁹ At higher temperatures, where the system obeys Boltzmann statistics, $D_\perp = D_\parallel = D_s$ and the above expressions are equivalent to Leggett's result, Eq. (1.2).

As is evident from the form of the above equations, all of the nonlinear effects are confined to the transverse spin dynamics. In a system where \mathbf{M} and gradients in \mathbf{M} are purely longitudinal, the spin dynamics remain completely linear. Gradients in M (which we may treat as a scalar in the purely longitudinal case) will simply relax according to the ordinary diffusion equation:

$$\frac{\partial M}{\partial t}(\vec{r}, t) = -D_\parallel \nabla^2 M(\vec{r}, t). \quad (1.6)$$

If one could develop a technique for measuring the coefficient of spin diffusion by exciting only longitudinal gradients, one could in principle measure D_\parallel independently of D_\perp (which could be obtained from a standard spin-echo experiment,^{20,21}) and thereby search for the predicted

diffusion anisotropy.

We have, in fact, developed such a technique for measuring D_{\parallel} in dilute ^3He - ^4He solutions, and in this paper we report on the results of that experiment. We also report on our investigations of the nonlinear transverse spin dynamics in the system, which include multiple spin echoes and a novel, extremely long-time-scale excitation. The next section of the paper is devoted to a discussion of our experimental techniques, including our method for determining D_{\parallel} . In Sec. III we give our results for D_{\parallel} in two different solutions, and compare them with recent theoretical calculations. Section IV contains a discussion of our multiple spin-echo experiments. In Sec. V we report on our observation of a new behavior in this system, with a characteristic lifetime on the order of 10 sec, and on our attempts to model that behavior with a simple computer simulation. Some of the results reported here have been previously published in a briefer form.²²

II. EXPERIMENTAL METHODS

A. General techniques

Experiments on spin-polarized ^3He - ^4He solutions require both low temperatures and high magnetic fields. For the experiments described in this paper, the former were provided by a large dilution refrigerator (Oxford Instruments) with a base temperature of ~ 3.5 mK. In order to reduce eddy current heating in the high-field regions, the cryostat was supported on a rigid platform of our own design with three high-performance vibration isolators (Technical Manufacturing Corporation). Vibrations transmitted along the refrigerator pumping lines were reduced by the installation of sandboxes and Kirk and Twerdochlib style double-gimbal isolators.²³ The requisite high magnetic fields for these experiments were provided by a 9-T superconducting solenoid (American Magnetics) with a 7.5-cm bore and a field homogeneity of better than one part in 10^6 over a 1-cm^3 region at its center.

We determined the sample temperature using a ^3He melting curve thermometer and the Greywall temperature scale.²⁴ Figure 1 offers a general schematic view of the apparatus, and shows the relative position of the melting curve thermometer and sample cell. The thermal link between the mixing chamber and the sample cell was made long enough so that the temperature error due to the residual magnetic field at the melting curve thermometer (<0.2 T) would be less than 0.5%.²⁵ The link was made from oxygen-free high-conductivity (OFHC) copper which had been annealed in an oxygen atmosphere ($\sim 10^{-4}$ Torr partial pressure) for 8 h at 800°C to improve its thermal conductivity. After the annealing, the copper had easily visible crystallites on the order of 1–2 mm in size. Because of the high specific heat of the copper nuclei in the 9-T field, the sample cell had a 5–6-h time constant at the lowest temperatures. As a result, we had to take particular care that the cell was in reasonable thermal equilibrium at the lowest temperatures. For our experiments on the higher concentration mixture,

we added a vibrating wire viscometer to the sample cell, which allowed us to more readily ascertain that the cell had come to equilibrium.

Also shown in Fig. 1 is our z gradient coil, which was designed to apply a large (~ 30 G/cm) uniform magnetic-field gradient $G = \partial H_z / \partial z$ to the sample cell. The coil was wound from Cu-clad multifilamentary Nb-Ti superconducting wire, and mounted on one of the thermal shields inside the refrigerator. The superconducting leads from the coil had their Cu cladding etched off in several places to reduce their thermal conductivity, and were brought out of the vacuum can and into the main bath space through an epoxy feedthrough.

The microwave cavity used in these experiments has been described in detail elsewhere.²⁶ Its design is based on the spit-ring resonator of Hardy and Whitehead,²⁷ but it employs a flexible metal-dielectric laminate that allows an extremely compact construction. It had a resonant frequency of 293 MHz, and a loaded Q of 1500 at low temperatures. The cavity was designed so that it could be tuned and coupled on a test rig that could be dipped into a helium storage Dewar, and then mounted onto the dilution refrigerator without further adjustment. Because of the large amount of power (~ 10 W) dissipated in the resonator during large tip angle pulses, it could not touch the sample cell. It was instead rigidly mounted close to the cell with low thermal conductivity Vespel rods (Dupont), and anchored to a higher-temperature stage of the refrigerator with a flexible copper braid.

While the high Q of the cavity allowed for an excellent NMR signal-to-noise ratio, it also resulted in a phenomenon known (somewhat misleadingly) as radiation damping.^{28,29} In this situation the field of the precessing spins, as amplified by the cavity, is large enough to react

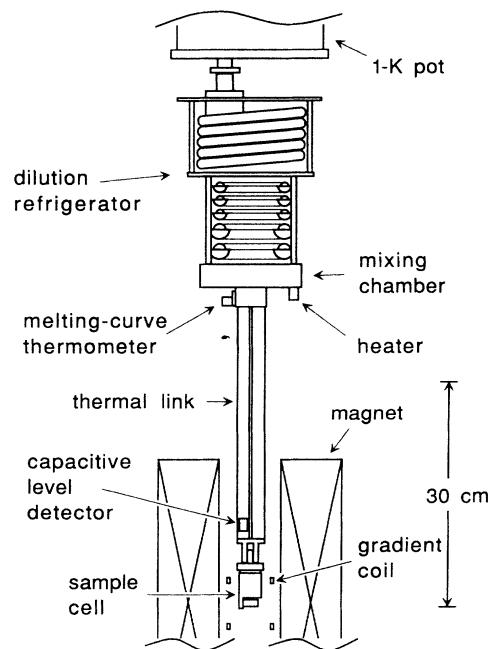


FIG. 1. Schematic view of the low-temperature portion of the experimental apparatus.

back on the spin system and exert a torque on the magnetization vector. While this effect is usually associated with higher-density spin systems, the low spin density in our experiments was more than compensated for by the high degree of spin polarization. For most of our experiments, the effect was quite small and only led to a NMR line shape that depended somewhat on both temperature and tip angle. At low temperatures in our higher-density sample the effect did become large enough that after a 180° pulse the sample magnetization vector was immediately rotated back to nearly its equilibrium direction. We were able to get around this difficulty by adjusting the current in our magnet so that the resonant frequency of the ^3He atoms was far enough outside the cavity linewidth to significantly reduce the effective Q of the cavity, and thereby reduce the radiation damping.

The broadband pulsed NMR spectrometer used in these experiments was of a conventional design, and was built largely from commercially available components. It has been described in detail elsewhere.³⁰

We prepared our ^3He - ^4He solutions by means of a mixing system in which the ratio of a small volume ($\sim 155\text{ cm}^3$) containing ^3He to a much larger one ($\sim 1.6 \times 10^4\text{ cm}^3$) containing ^4He had been carefully measured.³⁰ The sample concentration could then be determined from the initial pressure of ^3He in the small volume and the total pressure in the system once the two isotopes had been mixed. To minimize any errors that might result from an incomplete mixing, the total amount of sample was chosen so that, when liquified, it would only exceed the known sample cell volume by a small amount. The mixed sample was then drawn into a charcoal cryopump and loaded into the sample cell while the latter was held at about 1.5 K. As the sample loading progressed, the cryopump was gradually warmed so as to maintain a pressure of 1–2 bar at the top of the cell-fill capillary.

It is a well-known property of superfluid ^4He that any temperature gradient in the liquid will cause a supercurrent to flow toward the higher-temperature regions. In our mixtures, the resulting counterflow of normal fluid would sweep all of the ^3He to the coldest spot and distort the concentration of the sample. To prevent this “heat flush” effect, we placed a capacitive level detector (shown in Fig. 1) in the sample cell-fill line. The capacitor was mounted on the thermal link, quite close to the cell, and was carefully monitored during the cell-filling procedure. When the changing capacitance of the level detector indicated that the sample’s liquid-vapor interface was inside the detector, the filling procedure was halted, thus ensuring that none of the liquid extended up the fill line to warmer regions of the cryostat.

Two samples were prepared for the experiments described in this paper, one at a ^3He concentration of 350 ppm [$T_F = 13.3\text{ mK}$ (Ref. 31)], and a second at a concentration of 1940 ppm ($T_F = 41.4\text{ mK}$). As a check on the actual concentration, a portion of the mixed sample was transferred to a separate container and sent to the U.S. Bureau of Mines for analysis. Of the two samples sent for analysis, one was drawn from the completely mixed sample before loading any of the gas into

the sample cell. It was mixed to have a concentration of 1820 ppm, but was measured by the Bureau of Mines to have a slightly ($\sim 5\%$) higher concentration of $1940 \pm 40\text{ ppm } ^3\text{He}$. The portion of the 350-ppm sample sent for analysis was actually taken from the gas remaining after the sample had been completely loaded, so we would expect it to be somewhat depleted of ^3He (which, with its higher vapor pressure, would come out of the cryopump first). The sample analyzed by the Bureau of Mines had a concentration of $300 \pm 5\text{ ppm } ^3\text{He}$, but it is our judgment that the concentration in the actual liquid sample was most likely within 5% of 350 ppm. In a 9.2-T magnetic field, the “brute force” polarization at the cryostat base temperature of 4 mK is $\sim 65\%$ for the 350-ppm sample, and $\sim 25\%$ for the 1940-ppm sample.³²

B. Techniques for D_{\parallel}

Our technique for measuring D_{\parallel} is based on the method of Johnson *et al.*,^{8,33} who measured longitudinal spin diffusion in spin-polarized atomic hydrogen gas. The basic idea is quite simple. If we construct a sample cell with two chambers connected by a small channel, we can enclose one of these two chambers in a NMR coil or cavity. A π pulse applied to the cavity will then invert the spins in that chamber, and create a large *longitudinal* polarization gradient across the channel. Following the π pulse, spins will diffuse between the chambers until there is no longer any gradient, and the polarization in the two chambers will recover toward equilibrium. We can use the NMR cavity to apply small probe pulses and monitor this recovery as a function of time. If we can ignore T_1 (longitudinal relaxation) processes, then the recovery will be characterized by a single exponential time constant τ_0 that depends only on the geometry of the cell and the value of D_{\parallel} .

Of course, in any real experiment, the π pulse used to invert the magnetization will not be perfect, and will create some small amount of transverse magnetization. But because the applied static magnetic field is also not perfect, the transverse components in different parts of the cell will rapidly get out of phase, and—after a time T_2^* which is on the order of a few milliseconds—will average to zero. If the dimensions of the cell are chosen appropriately, τ_0 will be much longer than T_2^* , and any imperfections in the inversion will not matter.

A schematic drawing of the sample cell used in all the experiments described in this paper is shown in Fig. 2. The main body of the cell was constructed of Stycast 1266 epoxy (Emerson and Cuming). Thermal contact to the liquid was provided by a sintered silver heat exchanger with an area of approximately 25 m^2 . The heat exchanger, which also served as the lid of the sample cell, was of a conventional “post and hole” design.³⁴ The 700-Å silver powder (Vacuum Metallurgical Co.) used to make the sinter was pressed in four separate steps to a 50% (by weight) packing fraction and a total thickness of 10 mm.

In the experiment as we have described it so far, the measured quantity is the time over which the magnetiza-

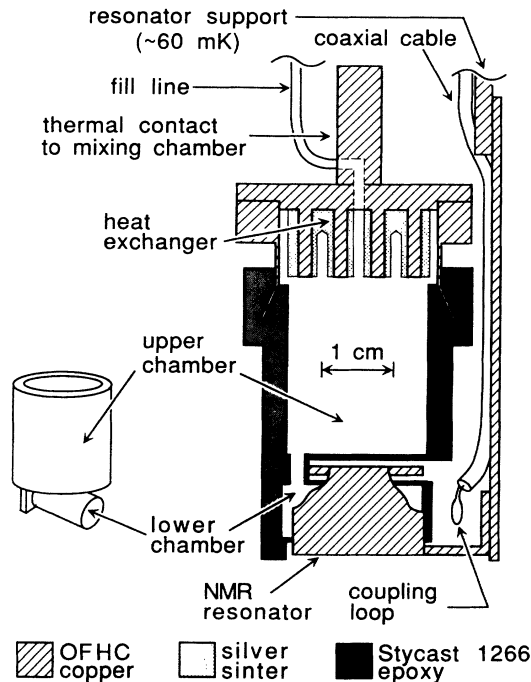


FIG. 2. Schematic view of the sample cell. The relative orientation of the upper and lower chambers is indicated by the smaller figure on the left. The NMR resonator is shown partly cut away. Note that the resonator and its support do not touch the cell.

tion in the lower chamber in Fig. 2 recovers to its initial value. To convert this time constant to a value for D_{\parallel} , we need to know the solution to the ordinary diffusion equation [Eq. (1.6)] for the cell. An exact analytical solution is quite likely impossible, given the complicated geometry of the cell. We can, however, easily find an approximate solution if, following Johnson,³³ we make a few simplifying assumptions. Initially following the inversion of the spins in the lower chamber (which we label volume 1), essentially all of the polarization gradient is along the length of the channel. Since the diameter of the channel is so small compared with the dimensions of the upper and lower cells, the gradient is likely to remain confined to the channel throughout the recovery, so it is not unreasonable to approximate the polarization as being completely uniform in the two chambers.

If we make the further approximation that the polarization is uniform across the diameter of the channel, and varies linearly along its length, then the total polarization flowing through the channel (per sec) is given by

$$I_M = D_{\parallel} \frac{\pi R^2 f}{L} (M_2 - M_1), \quad (2.1)$$

where M_2 is the (uniform) polarization in the upper chamber, R is the radius of the channel, and L is its length. The parameter f is a correction factor to take into account the fact that the gradients are not entirely confined to the channel. (Since we are assuming that any components of \mathbf{M} that do not point in the z direction in

spin space are small, we shall, for the moment, treat the polarization as a scalar quantity.)

If we can neglect T_1 processes (i.e., assume the total polarization in the cell is a conserved quantity), then any change in the polarization in the two chambers must be due entirely to the flow through the channel. It is then a straightforward matter to solve for M_1 as a function of time following a π pulse:

$$M_1(t) = M_f [1 - (1 + \epsilon) e^{-t/\tau_0}], \quad (2.2)$$

where M_f is the final polarization that both chambers relax toward, the polarization in the lower chamber at $t = 0$ has been defined as $M_1(0) \equiv -\epsilon M_f$, and the time constant for the exponential relaxation is given by

$$\frac{1}{\tau_0} = \frac{\pi R^2 f (V_1 + V_2)}{L V_1 V_2} D_{\parallel}. \quad (2.3)$$

Note that since $V_2 \gg V_1$, the time constant is relatively insensitive to the actual value of V_2 , and therefore insensitive to whether it includes the open volume in the silver sinter heat exchanger.

To find a value for f , which corrects for the finite length of the channel, we note that the spin-diffusion problem we are considering is mathematically identical to the problem of electrical conductivity, providing that D_{\parallel} is replaced by σ . In particular, if we model our cell as a small cylindrical wire connecting two semi-infinite electrodes, then we can use a result due to Maxwell³⁵ that the resistance of such a wire, including a "spreading resistance" correction for end effects, is given by

$$Z_e = \frac{L}{\pi R^2 \sigma} \left(1 + \frac{2\pi R}{3.82L} \right). \quad (2.4)$$

Comparison with Eq. (2.1) shows that the quantity in parentheses above is just f^{-1} . In our cell, $L/R \simeq 3$, so that $f \simeq 0.64$ and this correction for end effects is relatively large. Putting the actual values for the length and radius of the channel and the volumes of the two chambers into Eqs. (2.3) and (2.4) (see Table I), we find $D_{\parallel} \tau_0 = 13.03 \pm 0.56 \text{ cm}^2$, where the uncertainty is due to our uncertainty in the dimensions of the sample cell.

In arriving at the above result, we have made a number of approximations, some of which may have been quite severe. In particular, the analytical treatment of the cell assumes that the channel is nicely centered and accessible from all directions, and thus entirely determines the impedance between the two chambers. In the real cell, however, the channel is off to one side, very close to the walls, and so there must be some additional impedance associated with its position in the cell. In an effort to correct for this "corner effect," we used a Monte Carlo computer simulation to solve the diffusion equation in our exact cell geometry.

The basic approach used in the program was quite simple. The model sample cell was filled with 235 "sample" atoms, each labeled by a position and a spin. Initially, all the atoms in the upper chamber had spin $+1$, and all those in the lower chamber had spin -1 . For each run of the program, the initial positions of these atoms were chosen randomly from a uniform spatial distribu-

TABLE I. The sample cell dimensions used in calculating the value of $D_{\parallel}\tau_0$ given in Eq. (2.5). The larger uncertainty in V_2 reflects the uncertainty associated with whether or not to include the open volume in the sinter. It makes only a very small contribution to the total uncertainty quoted in Eq. (2.5).

V_1	$1.22 \pm 0.01 \text{ cm}^3$
V_2	$10.5^{+1.4}_{-0.2} \text{ cm}^3$
R	$0.122 \pm 0.003 \text{ cm}$
L	$0.36 \pm 0.01 \text{ cm}$

tion, and the resulting configuration was simply “random walked” toward equilibrium.³⁰ The averaged results of 75 such runs are illustrated in Fig. 3. There are four curves shown in the figure: the polarization in the upper and lower chambers as given by the simulation (solid lines) and the same two quantities as given by least-squares fits to the data from the *upper* chamber only (dashed lines). There appear to be only three curves in the figure because, on this scale, the simulated data and the fit for the upper chamber are indistinguishable. (The curve for the lower chamber is much noisier because it is derived from a much smaller number of atoms.) From that fit we obtain the final result

$$D_{\parallel}\tau_0 = 14.14 \pm 0.75 \text{ cm}^2, \quad (2.5)$$

which is about 8% larger than the analytic result quoted above. The inset in Fig. 3 shows the distribution of time constants obtained from fitting each of the 75 runs separately. The uncertainty quoted in Eq. (2.5) was obtained from the variance of this distribution and the uncertainty in our knowledge of the exact dimensions of the cell.

So far we have made only passing reference to what is actually a very important approximation in our treat-

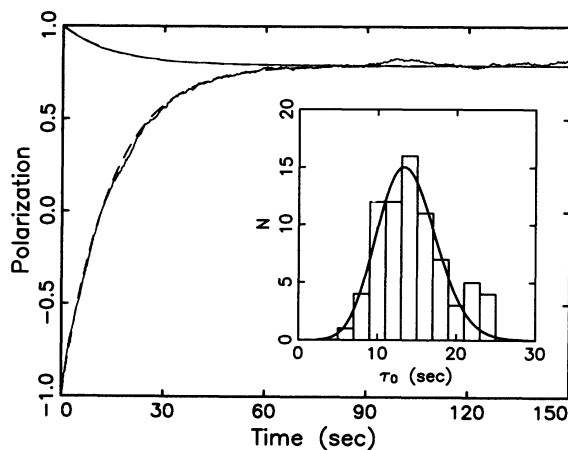


FIG. 3. Averaged results from 75 runs of a Monte Carlo solution of the diffusion equation in the sample cell. Shown are the polarizations in the upper and lower chambers. The dashed line is a single exponential recovery with a time constant determined from a least-squares fit to the data in the *upper* cell only. On this scale, the data from the upper chamber and its fit are indistinguishable. The inset to the figure shows the distribution of time constants obtained from fitting the 75 runs separately. The solid line is a fit to a Poisson distribution.

ment: we have been assuming that we can neglect all longitudinal relaxation processes. In both our analytic and numerical solutions of the diffusion equation, we assumed that the system would relax toward a final state in which the spins in the two chambers had completely mixed, but had not yet returned to thermal equilibrium. Our assumed final state has only $\sim 90\%$ of the polarization initially in the sample before the population in the lower chamber was inverted. True thermal equilibrium will be regained through longitudinal relaxation processes with a time constant T_1 , and the relative magnitude of T_1 and τ_0 will determine whether it is possible to correctly extract D_{\parallel} from our measurements. In particular, we require $T_1 \gg \tau_0$ in the lower chamber of the cell.

In principle, we could make a direct measurement of T_1 in our cell by saturating the spins in the lower chamber with a continuous string of 90° pulses. After a time $\sim 10\tau_0$, the magnetization in the upper and lower chambers would have completely exchanged, so that monitoring the recovery of the magnetization (once the 90° pulses have been stopped) should give T_1 . In practice, however, the relatively fast relaxation in the large surface area heat exchanger³⁶ makes it impossible for the slowly diffusing spins from the lower chamber to saturate the upper regions of the cell. We must instead rely on estimates of T_1 derived from the literature.

From the dimensions of our sample cell and the expected magnitude of the diffusion coefficient, it is easy to see that an atom will, on average, make several collisions with the cell wall during a time τ_0 . Therefore, we must consider relaxation processes that occur at the wall of the sample cell, as well as those that occur in the bulk liquid. If we consider the two processes to add in parallel, then the total relaxation time T_1 will be given by

$$\frac{1}{T_1} = \frac{1}{T_{1B}} + \frac{1}{T_{1W}}, \quad (2.6)$$

where T_{1B} and T_{1W} are the relaxation times associated with bulk and wall processes, respectively.

In liquids and gases, bulk relaxation occurs as a result of the dipolar interaction during the brief interval that a pair of colliding spins are within a scattering length of each other.³⁷ Quite recently, Mullin, Laloë, and Richards³⁸ reexamined this mechanism for the case of a quantum gas, and found that the relevant length scale is not the scattering length, but the thermal de Broglie wavelength of the atoms. Their results predict that for a 2000-ppm solution of ^3He in ^4He at 0.5 K, $T_{1B} \sim 4 \times 10^5$ sec, which is very much longer than our expected τ_0 . Since the dependence of their result on temperature and ^3He density is such that we would expect the relaxation time to become even longer at lower concentrations and lower temperatures, we may effectively neglect bulk processes in our consideration of T_1 .

The relaxation of ^3He nuclei at surfaces has long been considered anomalous and remains a problem without an adequate theoretical description (see Ref. 39 and references therein). It has been empirically determined, however, that T_{1W} depends linearly on the applied magnetic field,^{40,41} and that covering the surface with ^4He increases T_{1W} by a factor of 10–100.^{40,42} If we use the

data of Hammel and Richardson³⁹ for the T_{1W} of pure ^3He taken in the temperature range of our experiment and on a DLX6000 substrate,⁴³ and scale them to account for our much larger magnetic field and for the presence of ^4He in our system, we find that in the lower chamber of our sample cell $T_{1W} \gtrsim 10^7$ sec. Although this estimate is rough at best, it is significantly longer than either our estimate for the bulk relaxation time or our observed τ_0 . Taken together, our estimates for T_{1B} and T_{1W} give us a high degree of confidence that our measurements of τ_0 will not be significantly affected by relaxation processes.

III. LONGITUDINAL SPIN DIFFUSION

While our discussion and analysis of the sample cell and relaxation processes has been extended, the actual measurements of D_{\parallel} were quite straightforward. At a given temperature, we applied a π pulse to the spins in the lower chamber, followed by a series of 45 small probe pulses. The tipping angle of the probe pulses ($\frac{1}{2}^\circ$) was chosen to be sufficiently small so that their cumulative effect on the total polarization would be negligible. The free induction decay (FID) following each probe pulse was mixed down from 300 MHz to an audiofrequency ~ 10 kHz, digitized, and stored for later analysis. For reasons we shall discuss in Sec. V, these measurements were made with a small (~ 0.3 G/cm) magnetic-field gradient applied across the cell.

To obtain a number proportional to $M_z(t_n)$, where t_n is the time of the n th probe pulse in the series, we used a least-squares-fitting procedure. To prevent transients in the spectrometer electronics from affecting the results, the first 50 μsec of the FID were discarded and the fit was made to the next 2.5 msec of signal. The parameters obtained from the fit were then extrapolated back to obtain the signal amplitude at t_n . Because the lower chamber in the sample cell is somewhat larger than the manufacturer specified high homogeneity "region" in the center of the magnet, and because of the radiation damping contribution to the line shape we discussed earlier, we found it necessary to fit the signals to a sum of two exponentially damped cosines, which we did by a linear prediction technique.⁴⁴ The fits typically found a fast decay rate with a time constant on the order of 0.3 msec, and a slow decay with a time constant of 2–3 msec.

The 45 amplitudes were then fit to an exponential recovery of the form given by Eq. (2.2). Figure 4 shows a comparison of a typical recovery with its fit for data taken on a 1940-ppm solution. Also shown are the deviations from the fit. If the recovery were not well characterized by a single exponential, then the deviations should systematically lie to one side of zero around the "knee" of the curve, and to the other side at later times. Such behavior was not observed.

At each temperature, we averaged the results of four such recoveries to obtain a value for τ_0 from which, using Eq. (2.5), we computed D_{\parallel} . Figure 5(a) shows our results for D_{\parallel} between 4 and 400 mK in the 350-ppm solution. The error bars are derived from the fits and do not include the overall $\sim 5\%$ uncertainty in our value of $D_{\parallel}\tau_0$ that comes from the uncertainty in the exact cell geom-

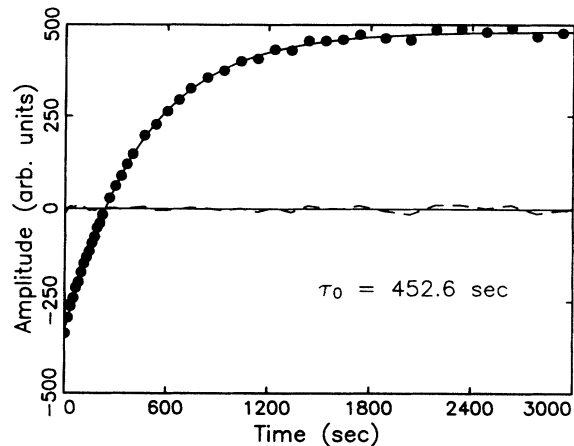


FIG. 4. The results of a single measurement of τ_0 in a 1940-ppm solution at 54.6 mK. The solid circles are the signal amplitudes following each of the 45 probe pulses, and the solid line is a least-squares fit to a single exponential recovery. The dashed line shows the deviations from the fit.

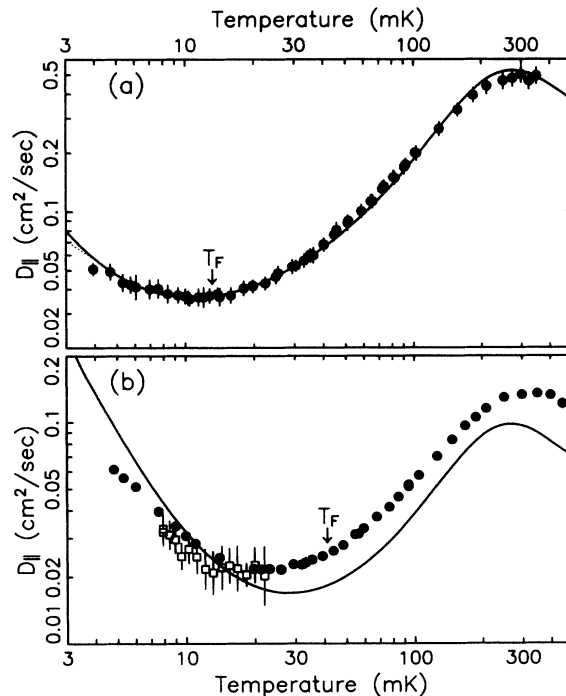


FIG. 5. Measured values of D_{\parallel} at 0 bar in a 9.2-T field (solid circles) compared with the calculation of Jeon and Mullin (Ref. 45) (solid lines) using the ^3He - ^3He potential of Ref. 46. The error bars shown are derived from the least-squares fits, and do not reflect the overall $\sim 5\%$ uncertainty in the product $D_{\parallel}\tau_0$. (a) Results for a 350-ppm solution. The dotted line at low temperatures indicates the predicted (Ref. 45) dependence of D_{\perp} at this concentration and magnetic field. (b) Results for a 1940-ppm solution. Also shown are the results of Candela *et al.* (Ref. 15) for D_{\perp} (open squares) in an 1840-ppm mixture.

etry and from the solution of the diffusion equation for the cell. Shown superimposed on the data is the theoretical calculation of Jeon and Mullin⁴⁵ appropriate to our field and concentration. The only parameter they have adjusted to improve the agreement between their theory and our experiment is the strength of the ^3He - ^3He interaction potential V_0 , which has been increased by about 4% over the value originally used by Ebner.⁴⁶ The main effect of this adjustment is a slight vertical shift in the calculated values of D_{\parallel} , but even without it, the agreement between our data and the calculation would still be well within the combined theoretical and experimental uncertainty.

In contrast to the results of the experiment by Gully and Mullin,¹⁶ we find that D_{\parallel} does in fact make a smooth transition between the expected high- and low-temperature behaviors, although we cannot quite reach low enough temperatures for D_{\parallel} to exhibit the $1/T^2$ behavior characteristic of a fully degenerate Fermi system.

An important limitation of this technique for measuring D_{\parallel} , which we have not so far discussed, is that our treatment of the sample cell assumes that the diffusion coefficient is uniform throughout the cell. In particular, since the polarization in the channel immediately after the inversion is a rapidly changing function of position, this technique requires that D_{\parallel} be, at most, weakly dependent on M , as has been pointed out by Bowley.⁴⁷ From a detailed comparison of Jeon and Mullin's calculations, which include mean-field effects, for $H = 9$ T and $H = 0$ T over the temperature range of our experiments, we find that the polarization dependence of D_{\parallel} only becomes significant below 10 mK, and even then, the predicted difference between $D_{\parallel}(0$ T) and $D_{\parallel}(9$ T) is much smaller than our uncertainty in $D_{\parallel}\tau_0$. Any attempt to extend these measurements to lower temperatures, however, may well have to take the polarization dependence of D_{\parallel} into account.

Since one of the original motivations for this experiment was to look for a discrepancy between D_{\parallel} and some independent measure of D_{\perp} , it would be nice, at this point, to be able to make a comparison between the two. As we shall discuss in Sec. IV, however, our attempts to measure D_{\perp} with a spin-echo technique were greatly complicated by the strong molecular field effects in the system. In addition, recent calculations by Jeon and Mullin,⁴⁵ shown as the dotted line at very low temperatures in Fig. 5(a), indicate that, for our 350-ppm solution, D_{\perp} should only be observably different from D_{\parallel} below the temperature range accessible with our current apparatus.

As an alternative approach to the problem of diffusion anisotropy, we decided to take advantage of the recent experiments by Candela *et al.*¹⁵ in which a spin-wave technique was used to measure μM and the quantity $D_{\perp}/\mu M$ in an 1820-ppm solution. While our attempt to match exactly that concentration missed by about 100 ppm, the difference between the Fermi temperature of our 1940-ppm solution (41.4 mK) and that of the solution studied by Candela *et al.* (39.7 mK) is negligible, given the resolution of our respective experiments.

Figure 5(b) compares our results for D_{\parallel} (solid circles) in the 1940-ppm solution with D_{\perp} as extracted from the data of Candela *et al.* (open squares). While at low temperatures their data fall consistently below ours, the uncertainties in both experiments are too large for us to claim that the discrepancy is due to diffusion anisotropy. In particular, while the difference between the data from the two experiments has the correct sign, and is slightly more than the theoretically predicted difference of 3–4% between D_{\parallel} and D_{\perp} ,⁴⁵ it is still less than the combined uncertainty of 7–10% from the two experiments.

Also shown in Fig. 5(b) is the same theoretical calculation of D_{\parallel} (with the same value of V_0) by Jeon and Mullin⁴⁵ as was compared with our 350-ppm results, but adjusted for the higher concentration. Although the data and theory have a similar temperature dependence, the quantitative agreement is not nearly as good as for the low-concentration experiment. The reasons for the discrepancy in this case are not understood. It is interesting to note that the two sets of experimental measurements seem to agree with each other better than either one agrees with the theory. It may be that the problem lies with the use of the Ebner potential to describe the ^3He - ^3He interactions; however, that potential was determined from experimental data at an even higher concentration (5%), and it would be very surprising to find that it did a poor job at 1940 ppm but worked again at 350 ppm. Further work, both experimental and theoretical, will be needed to resolve this disagreement.

IV. MULTIPLE SPIN ECHOES

A. Theory

Ordinary spin echoes are a well understood and widely used technique in magnetic resonance in which a pair of rf pulses (θ_1 and θ_2) applied to a system of spins at times $t = 0$ and $t = \tau$ result in a signal at $t = 2\tau$. The decay in the height of this "echo" signal as τ is increased can be used as a probe of spin diffusion in the system. Since the spin echo is built up from transverse magnetization created by the first pulse, the spin-diffusion coefficient determined from such a measurement will, of necessity, be D_{\perp} . It is easy to show (see, for example, Ref. 21) that if T_2 is sufficiently long, i.e., if transverse relaxation may be neglected, the height of the echo will be proportional to

$$e^{-2D^*/3} \equiv \exp[-\frac{2}{3}D_{\perp}(\gamma G)^2\tau^3], \quad (4.1)$$

where $G \equiv \partial H_0/\partial z$ is an applied linear gradient large enough to dominate any unknown contributions from imperfections in the magnet, etc. If the system is linear, then there will be no further echoes unless additional rf pulses are applied.

In systems with a strong molecular field, the simple behavior described by Eq. (4.1) no longer applies, as was first pointed out by Leggett and Rice.^{2,3} In particular, they showed that for the case that $\theta_2 = 180^\circ$, the dependence of the echo heights on the dimensionless parameter

$D^* = D_{\perp}(\gamma G)^2\tau^3$ is no longer exponential. Their predictions were fully verified by Corruccini *et al.*⁴ for the case of pure ^3He , but a similar experiment on a highly polarized ^3He - ^4He mixture by Gully and Mullin¹⁶ led to the anomalous results for both D_{\perp} and μM which we discussed in Sec. I.

If the second pulse in the sequence is not a π pulse, then the nonlinearities introduced by the molecular field can lead to the phenomenon of multiple spin echoes (MSE) in which *additional* echoes at times $t = n\tau$, $n = 3, 4, \dots$ appear in response to the original θ_1 - τ - θ_2 pulse sequence. Such multiple echoes are a fairly general phenomenon in which the nonlinear spin dynamics lead to a spatially modulated precession frequency. They were first observed in solid ^3He ,⁴⁸ and subsequently in both superfluid⁴⁹ and normal⁹ liquid ^3He , as well as in spin-polarized hydrogen gas.⁵⁰ Recently, they have even been observed in water at room temperature.⁵¹

In the case of solid ^3He , the nonlinear mechanism that drives the MSE results from a large internal dipolar demagnetizing field. Such a (considerably weaker) demagnetizing field is also responsible for the MSE observed in water. In their experiments on normal liquid ^3He , Einzel *et al.* found two regimes: a high-temperature one in which the multiple echoes were driven by a dipolar field, and a low-temperature regime in which the MSE were driven by an exchange molecular field. In the dilute solutions reported on here, it is this latter mechanism that is of interest; the spin density in these solutions is so low as to rule out any significant dipolar field effects.

The response of our 350-ppm sample to a 90° - τ - 90° pulse sequence is illustrated in Fig. 6. In this instance, in which the delay between the pulses was 1 msec, G (applied with the coil illustrated in Fig. 1) was 3 G/cm, and the temperature was 10.6 mK, there are 23 echoes visible. Note that although the second echo is large, successive echoes at first decrease in amplitude until, by the fifth echo, there is no signal at all. At later times the echo heights grow again and by the 12th echo are almost as large as the first multiple (i.e., second) echo.

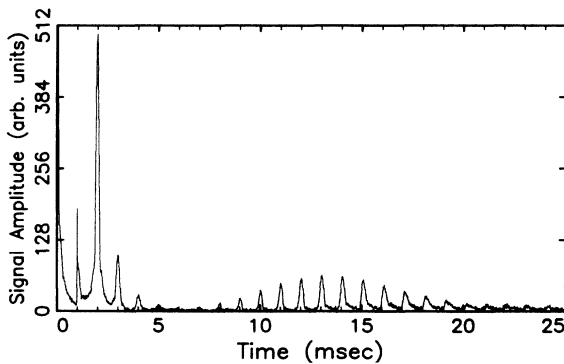


FIG. 6. Multiple spin echoes at 10.6 mK. The delay between the two 5- μsec 90° pulses was 1 msec, and the magnetic-field gradient in the z direction (parallel to H_0) was 3 G/cm. The signals at $t = 0$ and $t = 1$ msec are the free induction decays from the rf pulses. The remaining peaks are the spin echoes.

We may understand the origin of these multiple spin echoes in a very general way by briefly summarizing the analysis made by Einzel *et al.*⁹ The first rf pulse (which we will consider to occur at $t = -\tau$) creates a transverse component of magnetization which precesses in the applied magnetic field. Because of the large linear gradient included in that field, the magnetization will twist up into a helix along the z (magnetic field) axis in the sample cell. The pitch length of this helix at the time of the second pulse ($t = 0$) will be given by $l_p = 2\pi/\gamma G\tau$. Following this second pulse, the magnetization will have some complicated spatial structure, but will still have an underlying periodicity given by l_p . Since Einzel *et al.* expected the nonlinearities in the system to introduce higher harmonics of this periodicity, they sought a solution for the further time evolution of $M_+ = M_x + iM_y$ in the form of a power series in $\exp(i2\pi z/l_p)$:

$$M_+(z, t) = M_0 e^{-i\gamma G z t} \sum_{n=-\infty}^{\infty} A_n(t) e^{i\gamma G z n \tau}. \quad (4.2)$$

Any signal detected in the experiment will be a spatial average of M_+ over the volume enclosed by the rf cavity. From the two rapidly oscillating factors in Eq. (4.2), we can see that this average will generally be zero, *except* when t happens to be an integer multiple of τ . Then the precession term will be exactly canceled by the term in the power series with $n\tau = t$, and there will be a net signal (spin echo) whose amplitude is determined by the coefficient $A_n(n\tau)$. It is worth emphasizing that the form of Eq. (4.2) is quite general. All of the model-dependent parameters are manifested in the A_n , which can only be found by solution of the appropriate nonlinear equations for the spin dynamics.

For the case that both longitudinal and transverse relaxation processes can be neglected (i.e., T_1 and T_2 are very long compared to the duration of the echo train), Einzel *et al.*⁹ worked out analytic expressions for the A_n in two limiting cases. Of particular interest here is their result for the case in which the MSE arise from molecular-field (exchange) effects. They find that, providing $\mu M_0 \ll 1$, the height of the second echo is given by

$$A_2(2\tau) = \mu M_0 \sin^2 \theta_1 \sin \theta_2 (1 - \cos \theta_2) \times D^* \exp(-7D^*/3) \sum_{n=0}^{\infty} \frac{(-D^*)^n}{n!(2n+1)(2n+3)}. \quad (4.3)$$

Quite recently, Bedford *et al.*⁵² have rederived these results and have shown how the system may be treated numerically to obtain the echo heights when μM is not necessarily small, as well as when both dipolar and exchange mechanisms are important (as is the case in pure ^3He around 10 mK). They have also applied their results to experimental data on dilute ^3He - ^4He solutions⁵³ and find that, in the limit that $\mu M \lesssim 1.5$, the agreement between theory and experiment is very good.

Before turning to a discussion of our MSE data, we wish to emphasize that both the analytic result Eq. (4.3)

and the numerical results of Bedford *et al.* predict the echo heights to be a universal function of the parameter D^* . That is to say, if we compare spin-echo data taken at different magnetic-field gradients, all of the (properly normalized) heights obtained for the first (ordinary) spin echo should collapse onto a single curve if plotted against $G^2\tau^3$, which is proportional to D^* . Similarly, the second (first multiple) echo heights should lie on a single curve, and so on. In addition, the second echo height, as given by Eq. (4.3), should have a single maximum as a function of D^* .

B. Experiment

We obtained multiple spin-echo data using 90° - τ - 90° pulse sequences over a range of τ and a range of applied magnetic field gradients at several different temperatures. While we observed MSE in both the 350-ppm and 1940-ppm solutions, all of the results reported here were obtained from the lower concentration sample. We extracted the individual echo heights (which we denote E_1 for the first echo, E_2 for the second, etc.) from each digitized echo train, and normalized them to $E_1(0)$: the value of E_1 at $t = 0$ for that train. We obtained $E_1(0)$ by a backwards extrapolation of $\ln E_1$ against τ^3 .⁵² Although we could observe a second (i.e., first multiple) echo at temperatures as high as 60 mK, the MSE weakened relatively quickly with increasing temperature.

Figure 7(a) shows the results of our measurements of

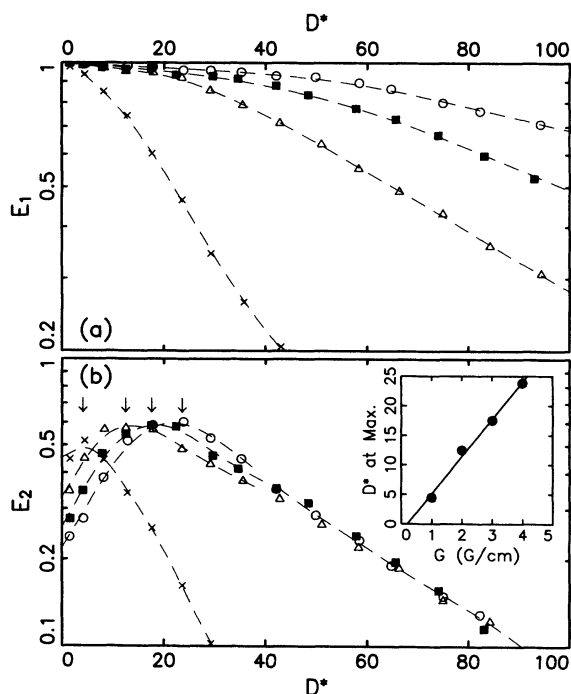


FIG. 7. Normalized (a) first echo and (b) second echo amplitudes as a function of the dimensionless parameter $D^* = D_{\perp}(\gamma G)^2\tau^3$ at 5.1 mK. The data shown were taken at the following magnetic-field gradients: $\times = 1$ G/cm, $\triangle = 2$ G/cm, $\blacksquare = 3$ G/cm, and $\circ = 4$ G/cm. The dashed lines are intended only as guides to the eye. Inset: The positions of the second echo maxima (indicated by arrows) as a function of field gradient.

the first echo amplitude at 5.1 mK for gradients of 1, 2, 3, and 4 G/cm. The parameter D^* was calculated according to Eq. (4.1) from the gradient, the delay, and our measured value of D_{\parallel} at that temperature. The dashed lines are intended only as guides to the eye. It is obvious that, contrary to the expectations discussed in Sec. IV A, the echo height data taken at different gradients do not fall onto a single curve. We also find that the data taken at the individual gradients do not fall onto straight lines, which indicates that the decay of the echo heights with increasing D^* is not exponential.

As we mentioned earlier, the latter is an expected result, and is due to the Leggett-Rice effect.^{2,3} An additional aspect of the Leggett-Rice effect is the “slowing down” of spin diffusion for the transverse components of the polarization. This slowing down is a direct consequence of the spin rotation (or molecular field) effects in the system. It has the effect of stretching out the time scale of the echo train since, roughly speaking, D_{\perp} in Eq. (4.1) is replaced by an “effective” diffusion coefficient

$$\tilde{D}_{\perp} = \frac{D_{\perp}}{1 + \mu^2 M^2}. \quad (4.4)$$

The importance of this effective diffusion coefficient can be seen in Fig. 7(b), which shows the behavior of the second echo at the same applied field gradients as in Fig. 7(a). The data taken at each gradient has only a single maximum as function of D^* , as predicted by theory. The positions of these four maxima (indicated by arrows) do not coincide, and they all occur at a much larger value of D^* than is predicted by Eq. (4.3), which has a maximum at $D^* \approx 0.4$. Since this equation is only applicable for small μM (i.e., for $\tilde{D}_{\perp} \simeq D_{\perp}$), it is apparent that the diffusion has indeed been slowed by the molecular field so that $\tilde{D}_{\perp} \ll D_{\perp}$. Since we have calculated D^* without taking into account this smaller effective diffusion coefficient, our data are “stretched” along the horizontal axis.

It seems, however, from the way in which the positions of the echo height maxima depend on G [see the inset to Fig. 7(b)], that this effective diffusion coefficient is a function of the applied gradient. There appears to be a similar effect in the way in which the expected universal dependence on D^* fails for the first echo [see Fig. 7(a)]. In both cases, the data taken at larger gradients appear to have a much smaller effective diffusion coefficient, which we see from Eq. (4.4) is equivalent to a much larger molecular field.

The amplitudes of the third and later echoes also exhibit somewhat unexpected behavior. Figure 8 shows the results of a high-resolution scan in which successive delay values were very closely spaced. The data were taken at 5.1 mK in an applied gradient of 4 G/cm, and show the normalized amplitude of the second, third, and fourth echoes, as a function of D^* . Note that while the second echo has a single broad maximum, the third echo has a sharp minimum, and the fourth echo has two. While these minima are not predicted by the analytic theory for small μM , the numerical treatment of Bedford *et al.* does in fact exhibit qualitatively similar behavior for large molecular fields ($\mu M \gtrsim 5$).⁵⁴

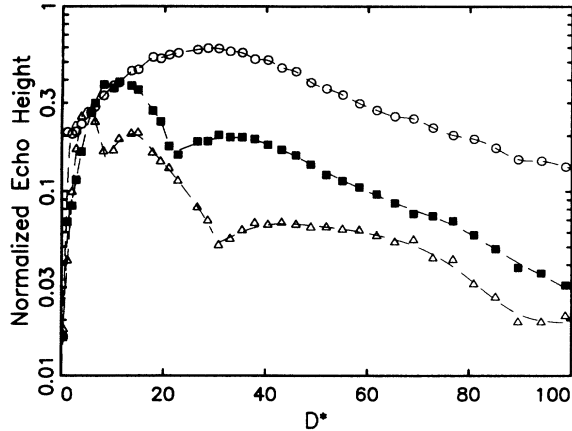


FIG. 8. High-resolution scan of the echo height as a function of D^* at 5.1 mK in a field gradient of 4 G/cm. The normalized heights of the second, third, and fourth echoes are shown as follows: $\circ = E_2$, $\blacksquare = E_3$, and $\triangle = E_4$. The dashed lines are intended only as guides to the eye.

While we would like to fit the results of Bedford *et al.* to our echo heights to obtain both D_{\perp} and μ , such an approach is bound to prove unfruitful, given the way in which our present data fail to scale with gradient and delay. Since the parameters of interest enter D^* approximately as the ratio D_{\perp}/μ^2 , a fit to the data at any one gradient would return values for D_{\perp} and μ which would be inconsistent with the data taken at other gradients. At this point, we have no way of determining which data set (if any) represents the “true” dependence on D^* .

A likely explanation for the nonuniversal behavior of the multiple spin echoes in our experiment can be found in the experiments of Owers-Bradley *et al.*,⁵³ who studied both MSE and the Leggett-Rice effect in ^3He - ^4He solutions where $\mu M \lesssim 2$. They found that they were unable to fit their results to the theory unless they took particular care to ensure that the magnetic-field gradient across the cell was extremely uniform, and that the cell diameter d was very small so that $Gd/H_1 \ll 1$. (H_1 is the rf magnetic field in the resonator during a pulse.) Even then, they found that they had to limit the magnetic field applied to the system so as to keep the polarization, and therefore μM , small. Otherwise, they found that, because of the spread in actual tip angle across the cell, M_z following a 90° pulse was not uniformly zero throughout the sample. As a result, there were *longitudinal* spin currents, which caused the magnitude of the polarization $|\mathbf{M}|$ to no longer have the same value everywhere in the cell.

Unfortunately, the analytic treatment by Einzel *et al.*⁹ requires a uniform $|\mathbf{M}|$ so that the quantity $\mu^2(\mathbf{M} \cdot \nabla \mathbf{M})$ in the Leggett equation [Eq. (1.2)] may be neglected. Without this simplification, the analysis of the echo heights becomes considerably more difficult. In their treatment, Bedford *et al.* developed a perturbative expansion for nonuniform $|\mathbf{M}|$, but it is limited to the case

that the nonuniformities are small. In our own experiment, the sample cell is very large, and the H_1 field in the resonator during a typical rf pulse is 15.5 G, so that in a 4-G/cm gradient, $Gd/H_1 \simeq 0.2$. During a nominally 90° rf pulse, the spread in actual tip angle across the cell diameter is 2° . The spin currents driven by the resulting gradients in M_z may not only explain the gradient dependence of our data, but may also explain the relatively slow decay of the echo heights (as compared to the theory⁵⁴) for longer τ .

For the moment, however, we remain unable to extract the physical quantity of interest, D_{\perp} , from MSE data taken in a cell designed for a measurement of D_{\parallel} . Future experiments to search for the predicted diffusion anisotropy will have to be done in an apparatus where particular attention has been paid to the uniformity of the gradient and tip angle. Even such a careful approach may encounter difficulties when the molecular field is large, as has been pointed out by Candela.⁵⁵ If the cell is made small so as to keep Gd/H_1 small, then, following a large angle tipping pulse, the spin currents driven by the $\mu \mathbf{M} \times \nabla \mathbf{M}$ term in the spin dynamics [obtained when Eq. (1.2) is substituted into Eq. (1.3)] will lead to the accumulation of M_z against one wall of the cell, and cause additional nonuniformities. While small-amplitude probes such as the spin-wave experiments of Candela *et al.*¹⁵ do not suffer from this difficulty, they are only sensitive to a linearized form of the spin dynamics. A well-controlled and correctly analyzed multiple spin-echo experiment would not only reflect the full form of the spin dynamics, but would also be sensitive to the presence of any diffusion anisotropy in the system.

V. LONG-TIME-SCALE OSCILLATIONS

A. Phenomenology

In our measurements of D_{\parallel} we probed the purely longitudinal spin dynamics of the spin-polarized ^3He - ^4He system. The behavior in this limit remains linear, and appears to be well described by theory. Our spin-echo experiments, on the other hand, primarily explored the nonlinear transverse spin dynamics. In this section we discuss our observation of a completely new, extremely long-lived excitation in this system. This excitation has a characteristic lifetime of about 10 sec—at least 2 orders of magnitude longer than that of weakly damped spin waves¹⁵—and appears to result from a situation in which a large-amplitude, but purely *longitudinal*, gradient in the magnetization becomes unstable against transverse perturbations. While the nature of these long-time scale oscillations are still not completely understood, we have developed a simple computer model that reproduces several key features of the observed behavior. Other aspects remain unexplained, however, and await further experimental and theoretical insight.

Figure 9 shows the digitized signal following a *single* π pulse applied to our 350-ppm sample at a temperature of 10.0 mK. The signal has been mixed down from 300 MHz

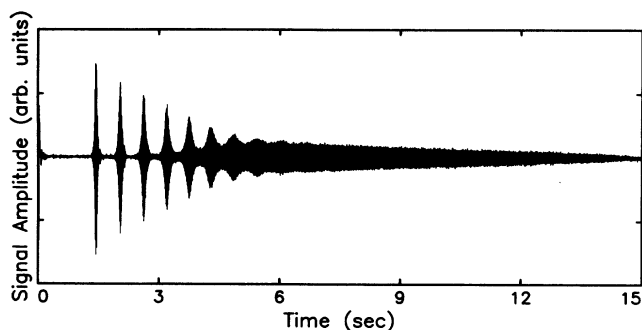


FIG. 9. Digitized free induction decay (FID) following a single π pulse at a temperature of 10.0 mK.

to about 80 Hz. The pulse was applied at $t = 0$, and because the population inversion was not perfect (due to small inhomogeneities in the rf and static fields), there is a short free induction decay (FID) as the net transverse magnetization dies away. After a *very* long delay of about 1.4 sec, during which the digitizer records only noise from the spectrometer electronics, the first of a series of sharp "bursts" suddenly appears. These bursts are at first separated by intervals in which there is again no signal, but gradually shrink in amplitude, broaden, and finally merge into a very long "tail" which can persist for as long as 16 sec after the initial π pulse.

Since this signal was mixed down to about 80 Hz and digitized at 500 Hz, the individual cycles of the signal are indistinguishable on this time scale, but are visible in the expanded view shown in Fig. 10. The well-defined oscillations confirm that these signals really do arise from a coherently precessing transverse magnetization. It bears repeating that this bursting behavior is the response of the system to a *single* rf pulse, not some multiple pulse sequence, so that the signal cannot be associated with any kind of spin-echo response.

We took great pains to ascertain that these signals were not an artifact, and in particular, not the result of rf "feedthrough" from the large-amplitude π pulse into the receiver portion of our spectrometer electronics. Because of the long-time scales involved, we could connect

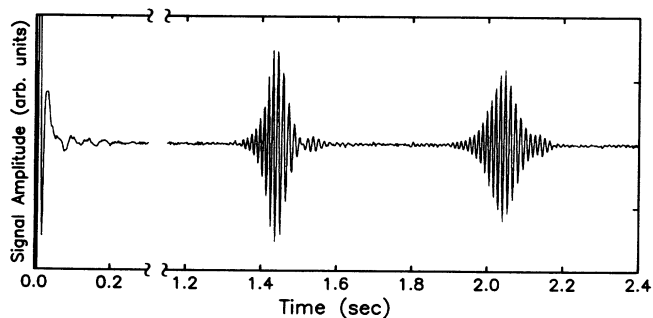


FIG. 10. Expanded view of the initial FID and first two "bursts" in the long-time-scale signal shown in Fig. 9. Note that these sharp features are part of the response to a *single* rf pulse, and are therefore unrelated to the spin echoes we would observe following a sequence of two or more rf pulses.

our power amplifier directly to the cryostat co-ax, apply the π pulse with the receiver section *completely* disconnected from the apparatus, and still have time to switch the cables and observe the latter part of the signal—a procedure which rules out recovery effects in both the amplifiers and the ferrite components of the spectrometer. As an additional check, we replaced the entire receiver system with a crystal diode detector and audio amplifier, and fed the output directly to an analog chart recorder. We again observed the long-time-scale signal, which gave us further confidence that this behavior was not an electronic artifact.

1. Tip angle, gradient, and temperature dependence

Of course, much more convincing support for the reality of these signals is provided by their sensitivity to experimental parameters that have little or nothing to do with the spectrometer. We found that the behavior appeared only if the pulse used to invert the spins was within about 20° of π . The results of a scan over a range of tip angles is illustrated in Fig. 11. Significantly, if the NMR pulse length was extended until the spins were swept through 2π , we did not get a signal, but if we rotated the spins by 3π , the signal reappeared. From these results we conclude that the driving mechanism for these signals depends on a complete, or near-complete, population inversion in the lower chamber of the sample cell.

All of the data shown in Figs. 9 and 11 were obtained with our magnet's shim coils adjusted to give as narrow a NMR linewidth as possible. Under these conditions the line shape was not particularly Lorentzian, but rather had a very sharp central peak on top of a much broader

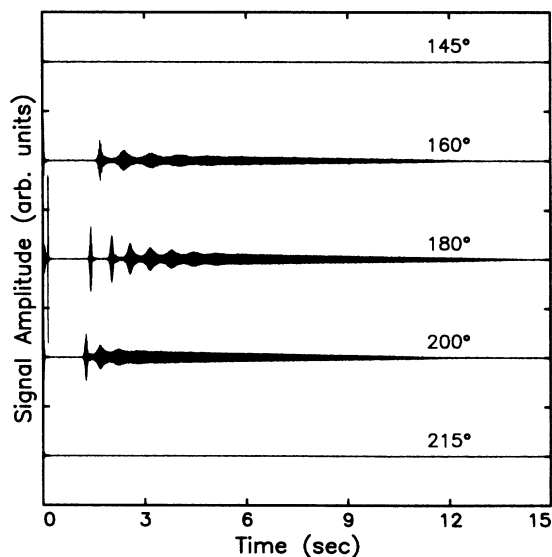


FIG. 11. Tip angle dependence of the long-time-scale oscillations at 10 mK. All of the data are drawn on the same scale. The data were taken with the magnet shim coils adjusted to give a "minimum gradient" (see text). Note the early burst (see text) that appears only for a tip angle of 180° .

background. If we added to this “minimum gradient” an additional, linear gradient, the change in the signal behavior was dramatic. Figure 12 shows the effect of adding a gradient parallel to the 9.2-T static field, and perpendicular to the long axis of the lower chamber. An increased gradient delays the arrival of the first burst, increases the interval between successive bursts, and suppresses the long tail. If the gradient is increased much beyond what is shown in the figure, the entire behavior disappears. If the gradient is instead applied perpendicular to H_0 and parallel to the long axis of the lower chamber, the behavior remains qualitatively the same. In both cases, if the field gradient across the cell is more than about 0.25 G/cm ($\Delta H \approx 3 \times 10^{-6}$ of H_0), the long-time-scale oscillations are completely suppressed, a fact which we used in our measurements of D_{\parallel} .

The signal traces in Fig. 12 also illustrate an additional, larger-amplitude burst at approximately 150 msec after the π pulse. We only observed this early burst at certain temperatures, and for particular configurations of the shim coils. In the case shown, this signal does not seem particularly sensitive to the additional linear gradient, although it is eventually suppressed at gradients $\gtrsim 0.4$ G/cm. Note that one of these early bursts appears in Fig. 11, but only for a 180° tip angle. When we applied the gradient perpendicular to H_0 , we did not observe this early burst at all. It is not yet clear how this early burst is related to the long-time-scale part of the signal. For the moment, it remains among the least understood aspects of the experiment.

The temperature dependence of these signals is quite dramatic, as is illustrated in Fig. 13. As the temperature

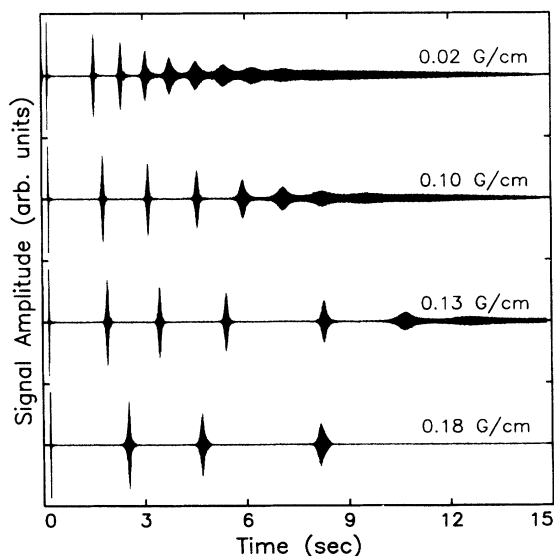


FIG. 12. Dependence of the long-time-scale oscillations on a magnetic-field gradient applied parallel to H_0 , and perpendicular to the long axis of the sample cell. The temperature is 9.9 mK. Note that the spacing between successive bursts is not even. The early bursts (see text) are clearly visible at $t \approx 150$ msec, and appear to have a uniform amplitude because they have all been clipped by the digitizer.

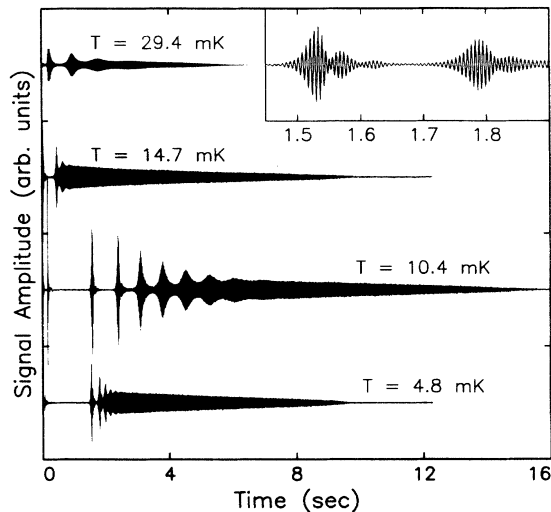


FIG. 13. Temperature dependence of the long-time-scale oscillations. All the data are drawn on the same vertical scale, and were taken using the “minimum gradient” configuration of the magnet shim coils (see text). The inset shows the part of the 4.8-mK trace between 1.5 and 1.9 sec on an expanded time scale.

is raised, the bursts become less pronounced and the overall time scale is reduced. For temperatures $\gtrsim 35$ mK, we do not observe these signals at all. The fact that they persist well above the Fermi temperature of this 350-ppm solution ($T_F \approx 13$ mK) suggests that the behavior is not driven by degeneracy effects. Note also that the strongest signals do not occur at the lowest temperature, but occur instead in the vicinity of 10 mK, where D_{\parallel} is at a minimum.

2. Size of the effect

Although these novel signals last for an extremely long time, their instantaneous amplitude is not very large. Comparison with the initial amplitude of the free induction decay following a 90° pulse shows that these signals are on the order of $\frac{1}{300}$ times as large. Because the signal from the NMR resonator represents a spatial average of the transverse magnetization over the whole lower chamber of the sample cell, we cannot tell from this comparison whether we are seeing a very small-amplitude disturbance across the whole cell, or one that has a large amplitude but is highly localized.

In either case, and in spite of the small instantaneous amplitude of the signals, the driving mechanism behind these oscillations eventually involves a substantial fraction of the spins in the lower chamber of the sample cell. We ascertained that this was the case by using a series of small-angle probe pulses—exactly as in our diffusion measurements—to determine M_z in the lower chamber immediately after the oscillation had died out. We compared these results with similar measurements in which an applied magnetic field gradient $\partial H_0/\partial z$ was used to partially or completely suppress the long-time-scale sig-

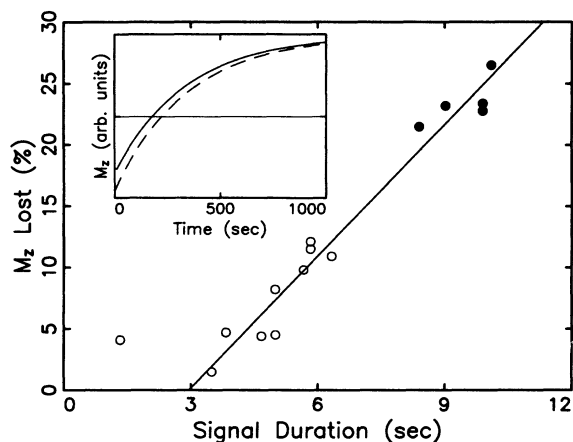


FIG. 14. Fraction of z component magnetization lost during a long-time-scale oscillation as a function of the duration of the signal. The data were obtained at 21 mK (\bullet) and 29 mK (\circ). The amount of lost magnetization is determined by comparing the recovery of M_z following the oscillation to the recovery observed when there is no long-time-scale signal, and is expressed as a percent of M_z immediately following the π pulse. Inset: a comparison of the “no signal” behavior (dashed line) with the exponential recovery following a 10-sec oscillation (solid line). Both curves were obtained at 21 mK.

nal. We found that after the oscillation had died out, the polarization in the lower cell was still largely inverted, but that the inversion was *smaller*, by as much as 25%, than it would have been in the absence of one of these signals. As can be seen from Fig. 14, the amount of z magnetization lost depends approximately linearly on the duration of the oscillation (or, to an equally good approximation, on the total rf power radiated during the signal). The important implication of this result is that these long-time-scale oscillations proceed by converting z component of magnetization into transverse components at a fairly steady rate, rather than by somehow preserving some initial transverse component created at the start of the oscillation. The fact that the amplitude of the signals remains small (instead of building as the oscillation progresses) implies that these transverse magnetization components are dissipated or otherwise destroyed as fast as they are created.

3. Additional features

While the sensitivity of these long-time-scale oscillations to such external parameters as field gradient and temperature is quite dramatic, there are some more subtle features of the data that are also worthy of note. One such feature can be seen in Fig. 10. There is a plainly visible frequency shift (~ 100 Hz) between the FID at early times, and the nonlinear oscillation at later times. This shift may be analogous to the frequency shifts observed in spin-wave experiments where the local molecular field causes the magnetization to precess at a frequency that is slightly different from the Larmor frequency. On the

other hand, it could simply indicate that the signal is generated in a relatively small region where the local Larmor frequency is somewhat different from the average over the whole cell. As we shall argue somewhat later, we believe that the second explanation is more likely.

In addition to this frequency shift, we find that the signals are also “chirped.” That is to say, the frequency of the oscillations is not constant in time, but shifts slightly over the length of the signal. This chirping is difficult to observe when the mixed down frequency of the signals is on the order of 100 Hz, but is clearly visible in signals which have been mixed to a much lower frequency.

We found that in order for the overall behavior of these signals to be reproducible, we had to wait until the sample had relaxed completely ($t \gtrsim 10\tau_0$) before applying successive π pulses, as is illustrated in Fig. 15. If we did not wait long enough, the signals appeared quite similar to those we observed when we applied a field gradient: the long tail of the signals was suppressed, and the time interval between successive bursts was extended. If we did allow sufficient relaxation, the overall behavior was largely reproducible, although there remained some trace-to-trace “jitter” in the exact arrival time of the bursts. This jitter likely indicates that there is some stochastic element to the driving mechanism behind these oscillations.

It is interesting to note that applying a second π pulse immediately after the signal died out did not shorten the time interval required for reproducibility. This second pulse returns M_z to nearly its equilibrium value,

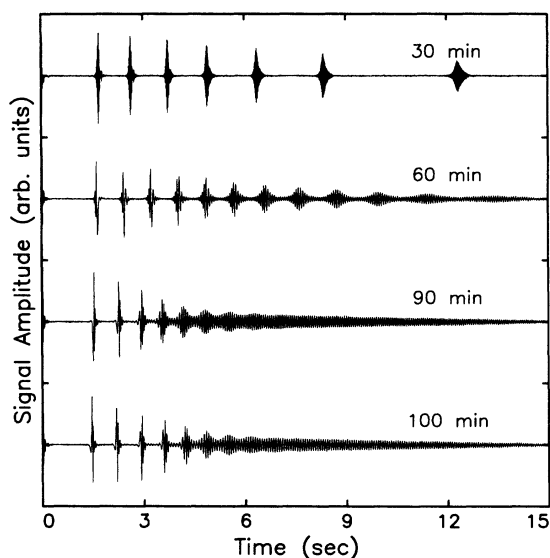


FIG. 15. Long-time-scale oscillations following π pulses separated by varying time intervals. Each trace is labeled by the approximate elapsed time since the previous pulse. Note that the upper two traces appear quite different from each other and from the lower two traces, but are very similar to the behavior seen when a field gradient is applied, as in Fig. 12. The lower two traces are nearly identical, and represent the response of the fully relaxed system. The apparent frequency of the signals varies because the ~ 75 Hz/h decay of the magnetic field has not been exactly compensated.

but cannot remove any residual transverse polarization created during the course of the oscillation. It seems, therefore, as if those residual components, although completely “scrambled” by inhomogeneities in the magnetic field, still have an important influence on the system, and that reproducible behavior is obtained only once all “memory” of the transverse magnetization has decayed away. In this liquid system, we expect that to occur on a time scale $T_2 \sim T_1$. If this argument is correct, it may also provide an explanation for the magnetic-field-gradient dependence. In that case, the transverse components of \mathbf{M} would be created by the spread in effective tip angle (due to the gradient), rather than a previous long-time-scale signal.

B. Radiative mechanisms

One of the first mechanisms we considered in searching for an explanation for these phenomena was some kind of maser oscillation or other stimulated emission effect. The characteristic time constant for such processes, however, is given by²⁰ $\tau_R = (2\pi\eta Q\gamma M_0)^{-1}$, where η and Q are the cavity filling and quality factors, respectively, γ is the ^3He gyromagnetic ratio, and $M_0 \simeq n_3\mu_3 M_0$ is the equilibrium magnetization of the spin system (n_3 and μ_3 are the ^3He density and nuclear magnetic moment, respectively). For our 350-ppm sample at 10 mK, this time constant is about 0.1 msec. If some kind of maser action were responsible for the long-time-scale oscillations, we would not only expect the process to start immediately after the π pulse when the cavity rf field is at its largest, but we would also expect it to exhaust the energy in the inverted spin system on a time scale given by τ_R . This is inconsistent with the long delay before these signals appear, with the overall time scale for the signals, and with our observation that there is still a substantial population inversion after the oscillation has died out.⁵⁶

A related mechanism we have also considered is not stimulated, but spontaneous emission. In this model, one imagines that any initial maser oscillation is somehow suppressed, but that after some delay, spontaneous emission causes the generation of an initial cavity field, which in turn causes stimulated emission and masing. Purcell⁵⁹ has shown that the spontaneous emission rate for a nuclear magnetic moment in a resonant cavity should be enhanced over the free-space rate by a factor that depends on the cavity volume V_c and quality factor Q . In our cavity ($Q \simeq 1500$, $V_c \simeq 2 \text{ cm}^3$), however, this enhancement factor is relatively modest, so the excited state lifetime is still on the order of 10^8 sec —much longer than either the initial delay or the subsequent signal observed in our system. As a result we do not consider either spontaneous emission or maser action to be plausible mechanisms for the generation of these long-time-scale oscillations.

C. A simple model

An important clue to the model that we have developed, and which does explain several aspects of the observed signals, is provided by an examination of the

temperature dependence illustrated in Fig. 13. As we pointed out earlier, the oscillations persist to well above T_F , and so are not likely a degeneracy effect. A more plausible mechanism is provided by the nonlinear terms in the spin-dynamical equations, whose strength is given by the parameter μM . An s -wave limit calculation of this parameter,¹⁸ which should be sufficiently accurate in this regime,⁴⁵ predicts that μM should remain significant (i.e., ≥ 1) up to temperatures on the order of 40 mK. On the other hand, this same calculation predicts that μM should diverge *roughly* as $1/T$, so that any nonlinear behavior should become stronger as the temperature is lowered. As can be seen in Fig. 13, however, that is not what happens. Instead, the signals with longest time scales and largest amplitudes are observed at intermediate temperatures in the vicinity of 10 mK. If the temperature is either raised or lowered from this point, the signals become shorter and the bursts become less pronounced (although at lower temperatures the initial delay does not shorten up).

There is a quantity, however, that does mimic the non-monotonic temperature dependence of these signals: the spin-diffusion coefficient. As can be seen from Fig. 5(a), the longest-time-scale oscillations occur near the minimum in D_{\parallel} , and shorter-time-scale signals appear to correspond to faster diffusion. For this reason, we believe that both the diffusion of M_z through the small channel between the two chambers in our sample cell, and the nonlinearities proportional to μM , play important roles in driving these signals.

If the observed behavior does indeed arise from some combination of spin diffusion and the inherently nonlinear spin dynamics in the system, then there must be some additional mechanism at work. After the π pulse, all of the polarization gradients are purely longitudinal, so the spin dynamics should remain entirely linear. In fact, all of our measurements of longitudinal spin diffusion were predicated on the fact that the spin configuration generated by the π pulse would *not* couple to the transverse nonlinear modes of the system. In order to invoke these nonlinearities as an explanation for the long-time-scale oscillations, we need a mechanism that will, under the right circumstances, generate transverse magnetization from initial conditions in which both \mathbf{M} and gradients in \mathbf{M} are purely longitudinal.

A mechanism that will provide precisely this coupling was actually pointed out some time ago by Castaing.⁶⁰ In an effort to explain some results from an experiment on rapidly melted spin-polarized ^3He , Castaing showed, via a simple linear stability analysis, that the Leggett equation has a regime in which small transverse perturbations will grow exponentially, instead of being damped. To illustrate how this mechanism may apply to our own experiment, we outline the relevant parts of his treatment below.

In the absence of a magnetic-field gradient, the spin dynamics of the system are given by Leggett’s equation for the spin currents, Eq. (1.1), and the continuity equation, Eq. (1.3), with $\delta\mathbf{H}$ set equal to zero. (Since we believe diffusion anisotropy to be unimportant at cur-

rently accessible temperatures, we shall consider the case that $D_{\parallel} = D_{\perp} \equiv D_s$.) We can examine the response of the system to small-amplitude perturbations by inserting into Eqs. (1.1) and (1.3) trial solutions which consist of the steady-state polarization and spin current plus a small oscillatory term:

$$\mathbf{M} = \mathbf{M}_0 + \mathbf{m}e^{i(\omega t - kx_1)}, \quad (5.1)$$

$$\vec{\mathbf{J}} = \vec{\mathbf{J}}_0 + \vec{\mathbf{J}}_1 e^{i(\omega t - kx_1)}. \quad (5.2)$$

Ordinarily, when such a procedure is carried out to obtain the dispersion relation for free (plane-wave) spin oscillations, the quantity $\vec{\mathbf{J}}_0$ is taken to be zero. That is to say, in the steady state, there are no spin currents. Following Castaing, however, we shall assume that there is, in fact, a large-amplitude steady-state spin current imposed on the system. By “steady state,” we mean only that this spin current is slowly varying on the time scales Ω_{int}^{-1} and ω^{-1} given by the molecular field precession and spin-wave frequencies, respectively, and on the length scale k^{-1} given by the spin-wave wavelength. What we have in mind as the origin of this spin current is, of course, the transport of magnetization through the channel that connects the two halves of our sample cell. It is driven by the “steady-state” gradient in the spin configuration following the π pulse, so we take this spin current to be carrying z component of magnetization, and to be defined by the relation

$$J_0^z = -D_s \vec{\nabla} M_0, \quad (5.3)$$

where M_0 is understood to be parallel to the z axis in spin space.

If we substitute the trial solutions including J_0^z into Eqs. (1.1) and (1.3), and keep only terms up to first order in the small quantities \mathbf{m} and $\vec{\mathbf{J}}_1$, it is a straightforward matter to find separate dispersion relations for the transverse and longitudinal components of the magnetization. For m_z we find

$$\omega_z = ik^2 D_s, \quad (5.4)$$

which describes ordinary spin diffusion. In other words, longitudinal perturbations remain purely damped, and their behavior is not affected by the addition of the large spin current. The result for $m_{\pm} \equiv m_x \pm im_y$, however, is somewhat different:

$$\omega_{\pm} = \frac{-k^2 D_s}{(i \pm \mu M_0)} \left\{ 1 \pm \frac{\mu}{k} \vec{\nabla} M_0 \right\}, \quad (5.5)$$

where we have used Eq. (5.3) to substitute for J_0^z . Aside from the factor in braces, Eq. (5.5) is just the dispersion relation for plane-wave spin oscillations.⁶¹

The importance of this additional factor, however, can be seen by considering what happens to Eq. (5.5) in the limit that gradients in M_0 are large enough that

$$\left| \frac{\mu}{k} \vec{\nabla} M_0 \right| > 1. \quad (5.6)$$

In this case, the entire dispersion relation would change sign. In particular, the imaginary part of Eq. (5.5) would

change sign, so that the amplitude of small *transverse* perturbations would grow exponentially instead of being damped.

This analysis forms the basis of our simple model for the long-time-scale oscillations. It shows that even from an initial condition in which \mathbf{M} and $\vec{\nabla} \mathbf{M}$ are purely longitudinal, it is possible for large gradients in the polarization to bring the spin dynamics into a regime where they are unstable against the growth of transverse components. Of course, in order for this to be a plausible model, the region of instability must correspond to the conditions of our experiment. We can approximate the gradient set up by the π pulse as $\vec{\nabla} M_0 \approx 2M/L$, where $L = 0.36$ cm is the length of the channel. If we estimate μM from Ref. 18 to be ~ 10 at 10 mK, and assume that k is determined by the characteristic dimensions of the lower chamber (~ 1 cm), then at 10 mK we find

$$\frac{2\mu M}{kL} \simeq 9 \gg 1, \quad (5.7)$$

so we are well within the unstable region. Given the same k and L , we find that there is a critical value of $\mu M \sim 1$ below which the instability will not occur, so that we should not expect to see the signals above approximately 30 mK, in reasonable agreement with what we observe in the experiment.

D. Computer simulations

The difficulty with the sort of linear stability analysis we have just carried out, however, is that, while it can show us that there *is* a region of instability, it can tell us nothing about the behavior inside the unstable region. We derived Eq. (5.5) in the limit of small perturbations, and what we learned is that the perturbations will not stay small. To investigate the behavior above the critical value of μM , we need to keep the full nonlinear equations for the spin dynamics. Because of the complicated form of these equations, we decided that the best approach was to model the system on a computer, and numerically integrate the time evolution of its spin dynamics.

1. Implementation

Because we hoped to recover the essential behavior of the system with as simple a model as possible, we chose to limit our simulation to one spatial dimension, and to work with a relatively small lattice of 128 points. While there are many algorithms for the numerical integration of diffusive equations that are designed to be both stable and fast,⁶² we found that adapting them to the more complicated Leggett equation did not seem promising. Instead, we decided to use a simple two-step explicit integration scheme in which we first calculated the spin currents, and then used the continuity equation to advance the system in time.

In order to mimic the flow of magnetization into and out of the lower chamber of our cell, we considered one end of the lattice to be connected to an infinite source of $M_z = +1$ and an infinite sink of $M_z = 0$. At the other,

“closed” end of the lattice, the boundary conditions were chosen so that there were no spin currents into or out of the wall. The entire simulation was carried out in the rotating frame, so that our simulated signals were automatically “mixed down” from 300 MHz.

For initial conditions, we tried to mimic the effect of an imperfect π pulse for $t \gg T_2^*$ by choosing M_+ to have a small uniform magnitude (typically, $|M_+| = 0.005$), but a random orientation, and by assigning $M_z = -1$ at every lattice site. The simulation was then simply allowed to propagate forward in time, and simulated signals were generated by periodically recording the average of M_x across the cell. Alternatively, the program could be made to record “snapshots” of the whole cell as a function of time.³⁰

In any numerical integration scheme, it is important to make sure that the calculation remains stable. In the present case, extra precautions were required because the system has an intrinsic instability, and we needed to ensure that any interesting behavior was associated with the true spin dynamics and not with a spurious numerical effect. In practice, we found it very easy to distinguish the two: in the latter case, the program would quickly start producing values of the polarization greater than 1. As a general rule, we encountered no difficulties if we stayed well within the stability criterion used in integrating ordinary diffusion equations.⁶² As an additional check, we verified that the program gave identical results with the time step reduced by half.

2. Results

Figure 16 shows a comparison of a simulated signal with an experimental signal taken at 5 mK and mixed to a very low frequency. The parameters used in the simulation correspond approximately to the experimental conditions. The model sample cell was taken to be 1 cm long, and the channel length was chosen to be 0.2 cm, to match the ratio 2 cm to 0.4 cm found in the actual cell. The diffusion coefficient was set equal to 0.05 cm²/sec, the amplitude of the initial, randomly oriented, transverse polarization was 0.005, and the equilibrium polarization was taken to be +1. There was a linear gradient

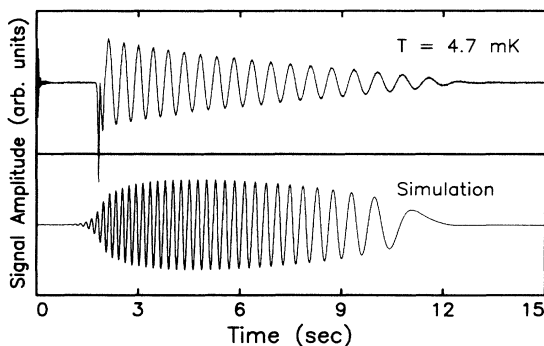


FIG. 16. Comparison of an experimental signal taken at 4.7 mK and a simulation. Note the monotonic frequency shift in both traces.

of -0.05 in units of $10^{-6} \times 9.2$ T/cm (≈ 0.045 G/cm) applied across the cell, and the point of zero frequency (in the rotating frame) was placed in the center of the cell. The spin rotation parameter μ was set equal to 7.0 so that μM would *roughly* correspond to the experimental value, at least as predicted by the *s*-wave limit calculation of Ref. 18.

In spite of the relative simplicity of our model, the simulations reproduce two of the most striking aspects of the experimental data: the initial delay after the π pulse, and the very long-time-scale signal that follows. The numerical signal even has a monotonic frequency shift similar to what is observed in the experiment. On the other hand, it does not exhibit any of the dramatic bursting behavior that is usually characteristic of the experimental signals.

While the comparison made in Fig. 16 looks quite reasonable, we cannot argue that our model does in fact describe the experiment unless we first verify that the numerical signals respond to such external parameters as magnetic-field gradient and temperature in a manner at least qualitatively similar to the actual long-time-scale oscillations, and that whatever triggers the oscillations in the simulation does in fact correspond to the Castaing instability on which our model was based. Only if the simulation seems to provide a plausible description of the experimental behavior can we use it to provide some insight into the internal dynamics of the system.

In order to test whether the numerical model does indeed respond in a manner similar to the experiment, we examined the simulated signals given by a broad range of input parameters. We found that as we increased the linear magnetic-field gradient, the simulated signals became smaller and shorter, and were eventually eliminated by a gradient of 0.05 G/cm. This gradient is only a factor of 2–4 smaller than the gradient required to eliminate the experimental signals, which we do not find unreasonable. On the other hand, increasing the gradient in the simulation leads to a shorter initial delay, in contrast to the experiment where increasing the gradient lengthened the initial delay.

Changing the “temperature” in the simulation is not quite as straightforward. In the actual experiment, both the strength of the molecular field and the speed with which the spins diffuse change with temperature. We found that since the sensitivity of the simulation to changes in these parameters does not exactly match the experiment, we could reach a better understanding of the behavior by varying D_s and μM separately. In the experiment, we found that increasing the diffusion coefficient (by moving the temperature away from the minimum in $D_{||}$ at ~ 10 mK) reduced the overall time scale of the signals, and (for temperatures above 10 mK) reduced the length of the initial delay. In the simulation we find a roughly similar behavior: speeding up the spin diffusion shortens both the initial delay and overall time scale of the signals.

Increasing the temperature in the experiment also results in a reduction in the strength of the molecular field μM , and a corresponding weakening of the long-time-scale oscillations. In our simulations, we find that the

signals are very sensitive to the value of μM , and that the correspondence to the experiment is somewhat rough. In the experiment, the signals disappear at a temperature where we estimate μM to be $\lesssim 2$. In the simulation, they disappear when $\mu M \lesssim 5$. If we increase μM , we find that a value of 7 gives a signal that is most like what is observed in the experiment. This value is about a factor of 2 smaller than the $\mu M \simeq 17$ at 5 mK we estimate from Ref. 18.

To verify that the growth of the simulated signals is in fact driven by the Castaing instability, we examined “snapshots” of the magnetization profile in the model cell at successive times. From the form of the critical parameter [Eq. (5.6)], it is apparent that the instability will be driven, at least initially, by long-wavelength (small- k) perturbations. Thus, we see that in order to drive the instability, the gradients in \mathbf{M} must be large (to make the critical parameter large) and must extend over long distances (to couple to long-wavelength perturbations). As a rough measure of this critical parameter, we constructed the quantity

$$\frac{\mu}{2\pi} \Gamma \left. \frac{dM_z}{dx} \right|_{x=0} \quad (5.8)$$

from the initial slope of M_z at the open end of the cell, and the distance Γ over which it fell halfway toward the value $M_z = -1$ far from the open end. We found that, although the initial slope was steadily decreasing with time, our “critical quantity” steadily increased, and had reached a magnitude of about 0.7 at $t = 1$ sec, where the signal first started to rise. Given the somewhat arbitrary definition of this quantity, we find the agreement with Eq. (5.6) to be reasonable.

Finally, if the behavior in the simulation really is governed by an instability in the spin dynamics, then we would expect the results to be only weakly dependent on the perturbation that seeds the initial growth. In our simulation, that perturbation is provided by the randomly oriented transverse component of \mathbf{M} which we assigned to each lattice site at $t = 0$. We found that neither using a different random orientation nor reducing the amplitude of the initial M_+ by a factor of 10 had a significant effect on the simulations. In both cases, the amplitude, initial delay, and overall time scale of the signals remained quite close to those illustrated in Fig. 16.

3. Analysis

Since the general behavior of our simulation in response to such parameters as the magnetic-field gradient and temperature approximately follows that of the experimental signals, it seems reasonable to believe that a more detailed examination of the internal dynamics of our model system will give us some insight into the actual long-time-scale oscillations themselves.

Figure 17 shows a “snapshot” of the magnetization along the length of the cell at $t = 4$ sec for the simulation illustrated in Fig. 16. The dotted line shows the profile that M_z would have if there were no nonlinearities in the system ($\mu = 0$). The solid line shows the actual

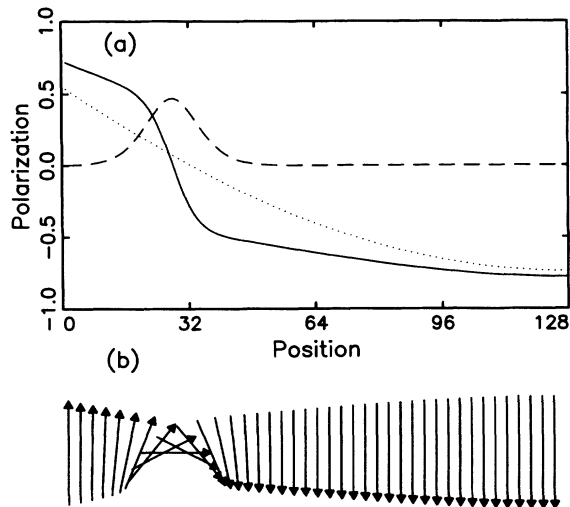


FIG. 17. (a) A “snapshot” of the polarization inside the cell at $t = 4$ sec for the simulation illustrated in Fig. 16. The open end of the 1-cm-long cell is at lattice position 0, and the closed end is at lattice position 128. The dotted line gives M_z for the case that $\mu = 0$, while the solid line gives M_z for the case that $\mu = 7$. The dashed line shows $|M_+|$ (for $\mu = 7$) and is plotted on the same scale as the other curves. (b) A vector plot of the total polarization across the cell showing a coherent “twist” in \mathbf{M} .

profile of M_z , which exhibits a region with an extremely steep gradient. Note that the value of M_z at the open (left-hand) end of the cell is *higher* than it would be in the absence of the nonlinear terms, and therefore slows down the rate at which spin-up polarization can enter the cell. Also shown in the figure (dashed line) is the magnitude of the transverse polarization, which is zero everywhere in the cell except in the region of steep gradient in M_z . Both M_z and $|M_+|$ are plotted on the same scale, so it is evident that the transverse component is large.

Even more intriguing is the vector sum of the two quantities, also illustrated in Fig. 17. It shows that the magnetization develops a sharp, coherent 180° twist that forms a domain-wall-like boundary between the spin-up and spin-down regions of the sample cell. The signal in the simulation comes entirely from the transverse component of \mathbf{M} in the region of the twist, which perhaps answers one of our questions about the experimental behavior. In the simulation, at least, the signal arises from a large-amplitude disturbance in a small region of the cell, rather than from some small disturbance over the whole cell.

Further insight into the behavior of the simulation can be gained by considering the time development of the magnetization across the whole cell. Figure 18 shows the profile of M_z at 1-sec intervals (for the same set of parameters as in Fig. 16). At early times, before the growth of the instability, the polarization, as a function of distance along the cell, just smoothly decays from its value at the open end. At some point, however, it starts to develop a small kink. The kink then appears to act

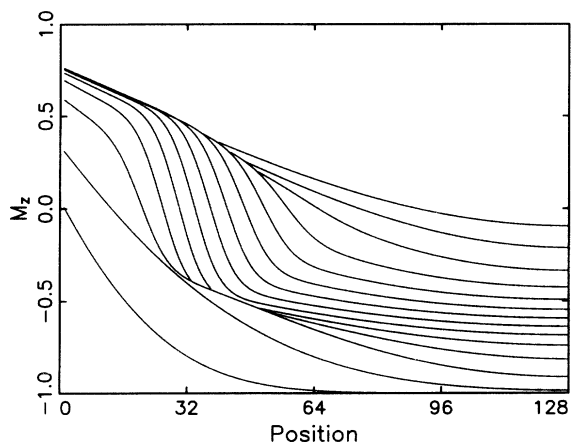


FIG. 18. A time series showing the profile of M_z across the cell at 1 sec intervals. The data correspond to the simulation shown in Fig. 16.

back on itself (through the transverse components of \mathbf{M}) and to continue to steepen until it reaches some limiting slope. As the simulation progresses, however, ordinary spin diffusion continues to drive spin-up polarization into the cell, so that the value of M_z on the “downstream” side of the kink continues to rise. Eventually the polarizations on either side of the steep region become too close in value, the gradient is forced below the critical point, and the kink dies out.

Figure 19 shows a matching time series, but at half-second intervals, for the magnitude of M_+ . At early times, there is no net transverse magnetization in the cell, but as the kink in M_z (which actually corresponds

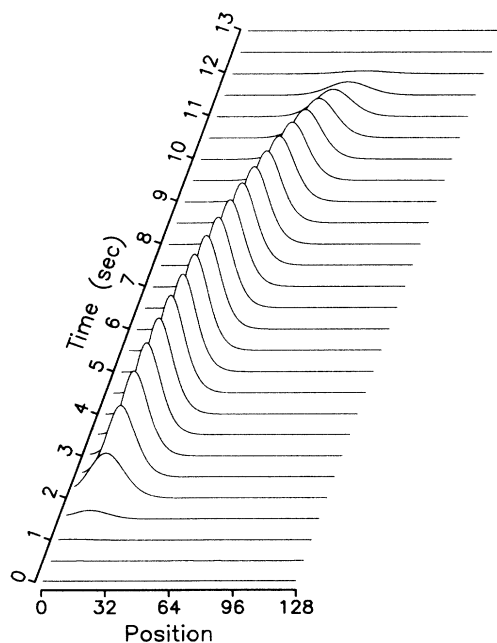


FIG. 19. A time series showing the profile of $|M_+|$ across the cell at half-second intervals. The data correspond to the simulation shown in Fig. 16.

to a twist in the vector \mathbf{M}) develops, M_+ starts to build up. The twist then moves down the sample cell and eventually dissipates, which may provide us with another clue to the behavior observed in the experimental signals. In the simulations, at least, the frequency shift or “chirping” arises from the change in the local Larmor frequency (due to the applied magnetic field gradient) as the “domain-wall” structure moves down the cell. The fact that the signal dies out just as it reaches the point of zero frequency (see Fig. 16) is coincidental. Moving that point both closer to and farther from the open end of the cell had no effect on the envelope of the signal.

The behavior illustrated so far raises several additional questions, including to what degree the duration of the signals depends on the size of the cell. As can be seen from Fig. 18, the signal dies out when there is not enough “headroom” between the values of M_z on the upstream and downstream sides of the domain wall, so that we might expect a bigger cell to result in a longer signal (since there would be more room for the polarization on the downstream side to spread away from the kink). In a (simulated) 5-cm cell, the signal is indeed longer, but not enormously so (16 sec instead of 12). In fact, examination of the magnetization profile in that case revealed that when the signal died out, the domain wall had only traveled about 0.5 cm into the cell. Most of the magnetization in the cell was undisturbed, so that the closed end of the cell had no effect on the duration of the signal. The behavior of M_z in the vicinity of the kink, however, looked almost identical to the behavior illustrated in Fig. 18. In other words, even without a wall to confine the polarization, M_z on the downstream side of the kink still rises up and pinches off the signal.

It appears from the long cell results that the duration of the signal is controlled by the relative strength of the reactive terms in the spin dynamics, which form the kink and cause it to sharpen up, and the dissipative terms, which work to spread the kink out. By increasing μ , we could increase the importance of the reactive terms, in which case the kink became much steeper and persisted for a much longer time. It is also interesting to note that with an increased μ , the kink traveled down the cell much more slowly. The reason for this reduced motion is found in Fig. 17 where we pointed out that the appearance of the domain wall raised the value of M_z at the open end of the cell. Our simulations show that an increased μ is even more effective at this, further slowing the rate at which polarization can enter the cell and push the domain wall downstream.

Given the limitations of our model, the best description of our results so far is that they are suggestive. We find it likely that the actual long-time-scale oscillations observed in the experiment are driven by a nonlinear instability in the Leggett equation, but there remain several unresolved issues. The question of what drives the “bursting” behavior is among the most interesting of these.

Also of interest is the relation, if any, between the behavior revealed in our simulation and the previously investigated spin dynamics in this system. In particular, Lévy⁶³ has shown that in the limit of very low dissipation

(i.e., for μM sufficiently large) the Leggett equation can be decoupled into separate equations for the magnitude of the magnetization, M , and its direction, $\hat{\ell}$. The former just obeys the ordinary diffusion equation, but $\hat{\ell}$ obeys the Heisenberg ferromagnet equation, which has known spin-wave, soliton, and soliton wave train solutions.⁶⁴ Lévy showed that in the next approximation, the equation for $\hat{\ell}$ includes an additional dissipative term. In this case, he found that the spin dynamics include not only spin waves and solitons but also more complicated three-phase modes termed “pulsions.” All of these behaviors, however, were found in a regime where the system had been stabilized against transverse perturbations by the application of a linear magnetic-field gradient. In our experiment, the long-time-scale signals are *suppressed* by a field gradient, and in our model, it is just such a transverse instability that drives the entire behavior. It seems at least plausible that the behavior we observe is precisely the sort of instability that Lévy wished to avoid in his analytic treatment of the spin dynamics.

Finally, we note that although we searched for these long-time-scale signals in our more concentrated (1940 ppm) mixture, we were unable to observe them. It appears that the combination of reduced polarization and (slightly) slower diffusion prevents the system from exceeding the instability criterion. If we put the appropriate parameters into our simulation, we find that there is an instability, but it only sets in after about 10 sec. We find it extremely unlikely that in the real cell, where gradients can spread out in three dimensions, an instability would occur after such a long time.

We have also searched for the nonlinear behavior reported by Owers-Bradley⁶⁵ in which a periodic ringing signal was observed for up to 10 msec following a pair of very closely spaced 90° pulses, but could find no evidence for a similar behavior in our experiment.

VI. SUMMARY AND CONCLUSIONS

In summary, we have measured the coefficient of longitudinal spin diffusion in dilute ^3He - ^4He solutions with ^3He concentrations of 350 and 1940 ppm. In both the high- and low-concentration mixtures, we find that our data smoothly cross over from a high-temperature regime where D_{\parallel} *decreases* with decreasing T to a low-temperature regime where D_{\parallel} *increases* with decreasing T . In neither case did we observe behavior similar to that seen by Gully and Mullin at low temperatures.¹⁶ For the lower concentration, the agreement between our measured values of D_{\parallel} and theoretical calculations⁴⁵ is excellent. The lack of equally good agreement in the higher-concentration case remains something of a puzzle. In addition, we have been able to compare our results for D_{\parallel} in the 1940-ppm solution with Candela *et al.*'s results¹⁵ for the coefficient of transverse spin diffusion D_{\perp} . Within the combined experimental error of the two sets of data, we do not observe a significant difference

between D_{\parallel} and D_{\perp} , which is consistent with theoretical predictions for this relatively high-temperature regime.⁴⁵

Our attempts to measure D_{\perp} with a spin-echo technique were less successful. While the strong multiple spin-echo behavior we observed confirms the presence of large molecular fields in the system, the lack of agreement between our data and theoretical predictions, and, in particular, the failure of the echo amplitudes to scale as expected with field gradient and interpulse delay, prevented us from measuring both D_{\perp} and the spin rotation parameter μ directly. For the moment, we consider it likely that rf and static magnetic field inhomogeneities across our relatively large sample cell are the source of the discrepancies. If such experimental difficulties could be surmounted, however, the technique of multiple spin echoes promises to be a powerful tool for the investigation of highly polarized systems. They are a large-amplitude probe that should be sensitive to the existence of the as yet unobserved diffusion anisotropy, and should provide information about the exact form of the spin dynamics in the highly polarized regime. This last point is particularly important, as such information cannot be obtained from spin-wave experiments and other small-amplitude probes that are only sensitive to the linearized spin dynamics of the system.

Finally, we have observed a very long-time-scale excitation in the system which we believe is driven by a nonlinear instability in the spin dynamics. While we have developed a simple computer model that reproduces some key aspects of this behavior, our understanding of this phenomenon is still somewhat preliminary. Examination of the spin dynamics in the simulated sample cell indicate that the experimental signals may have their origin in a “half-soliton”-like mode, but it is important to emphasize that we are still uncertain as to what extent the computer model actually describes our experiment. While we are able to generate numerical signals whose overall time scale matches that of the experiment, and which depend on such external parameters as magnetic-field gradient and temperature in roughly the correct fashion, we are unable to reproduce the dramatic “bursting” behavior observed in the experiment.

It is clear that much work, both experimental and theoretical, remains to be done in order to fully understand this behavior. Any future simulations should incorporate more spatial dimensions. If the bursting behavior depends in some fashion on the geometry of the channel, it may appear in a two- or three-dimensional simulation that can more accurately describe the spin dynamics in all three regions of the sample cell. It may also be possible to find a solvable analytical treatment in the unstable region, which would likely offer more insight than a simple numerical integration. From an experimental point of view, since we believe the driving mechanism for these oscillations depends on the flow of spins through the small channel in the cell, it would be extremely interesting to be able to control that flow by changing the cell geometry (e.g., with a movable partition) from outside the cryostat. Attempting to alter the behavior during the course of the oscillation by, for example, applying a pulsed gradient, may also prove revealing.

ACKNOWLEDGMENTS

We are grateful to W. J. Mullin for providing us with theoretical calculations of D_{\parallel} for our concentration and field, and to D. Candela for providing us with his data on D_{\perp} . We thank both of them, as well as J. P. Sethna, A. S. Bedford, R. M. Bowley, J. R. Owers-Bradley, and J. H. Freed, for stimulating and helpful discussions. We

are also grateful to R. W. Nelson and S. A. Teukolsky for help with our simulations of the long-time-scale oscillations, and to E. N. Smith for help with the apparatus. This work was supported by the NSF under Grant No. DMR-9011562 and through the Cornell Materials Science Center via Grant No. DMR-8818558-A02. We gratefully acknowledge the support provided to G.N. by IBM Research Division, to A.M.P. by NSERC of Canada, and to D.L.H. by AT&T Bell Laboratories.

*Present address: IBM Research Division, T. J. Watson Research Center, Yorktown Heights, NY 10598.

¹For a review, see *Spin Polarized Quantum Systems*, edited by S. Stringari (World Scientific, Singapore, 1989); A. E. Meyerovich, in *Helium Three*, edited by W. P. Halperin and L. P. Pitaevskii (North-Holland, Amsterdam, 1990).

²A. J. Leggett and M. J. Rice, *Phys. Rev. Lett.* **20**, 586 (1968).

³A. J. Leggett, *J. Phys. C* **3**, 448 (1970).

⁴L. R. Corruccini, D. D. Osheroff, D. M. Lee, and R. C. Richardson, *Phys. Rev. Lett.* **27**, 650 (1971); *J. Low Temp. Phys.* **8**, 229 (1972).

⁵E. P. Bashkin, *Pis'ma Zh. Eksp. Teor. Fiz.* **33**, 11 (1981) [*JETP Lett.* **33**, 8 (1981)].

⁶C. Lhuillier and F. Laloë, *J. Phys. (Paris)* **43**, 197 (1982); **43**, 255 (1982); C. Lhuillier, *ibid.* **44**, 1 (1983).

⁷L. P. Lévy and A. E. Ruckenstein, *Phys. Rev. Lett.* **52**, 1512 (1984); A. E. Ruckenstein and L. P. Lévy, *Phys. Rev. B* **39**, 183 (1989).

⁸B. R. Johnson, J. S. Denker, N. Bigelow, L. P. Lévy, J. H. Freed, and D. M. Lee, *Phys. Rev. Lett.* **52**, 1508 (1984).

⁹D. Einzel, G. Eska, Y. Hirayoshi, T. Kopp, and P. Wölfle, *Phys. Rev. Lett.* **53**, 2312 (1984).

¹⁰N. Masuhara, D. Candela, D. O. Edwards, R. F. Hoyt, H. N. Scholz, D. S. Sherril, and R. Combescot, *Phys. Rev. Lett.* **53**, 1168 (1984); D. Candela, N. Masuhara, D. S. Sherril, and D. O. Edwards, *J. Low Temp. Phys.* **63**, 369 (1986).

¹¹J. R. Owers-Bradley, H. Chocholacs, R. M. Mueller, Ch. Buchal, M. Kubota, and F. Pobell, *Phys. Rev. Lett.* **51**, 2120 (1983); J. R. Owers-Bradley and R. M. Bowley, *J. Low Temp. Phys.* **63**, 331 (1986).

¹²H. Akimoto, T. Kawae, G-H. Oh, O. Ishikawa, T. Hata, T. Kodama, and T. Shigi, *Jpn. J. Appl. Phys.* **26-3**, 65 (1987).

¹³H. Ishimoto, H. Fukuyama, N. Nishida, Y. Miura, Y. Takano, T. Fukuda, T. Tazaki, and S. Ogawa, *Phys. Rev. Lett.* **59**, 904 (1987).

¹⁴P. J. Nacher, G. Tastevin, M. Leduc, S. B. Crampton, and F. Laloë, *J. Phys. Lett. (Paris)* **45**, L441 (1984).

¹⁵D. Candela, D. R. McAllaster, L-J. Wei, and G. A. Vermulen, *Phys. Rev. Lett.* **65**, 595 (1990); D. Candela, D. R. McAllaster, and L-J. Wei, *Phys. Rev. B* **44**, 7510 (1991).

¹⁶W. J. Gully and W. J. Mullin, *Phys. Rev. Lett.* **52**, 1810 (1984).

¹⁷A. E. Meyerovich, *Phys. Lett.* **107A**, 177 (1985).

¹⁸J. W. Jeon and W. J. Mullin, *J. Low Temp. Phys.* **67**, 421 (1987).

¹⁹J. W. Jeon and W. J. Mullin, *J. Phys. (Paris)* **49**, 1691 (1988); *Phys. Rev. Lett.* **62**, 2691 (1989).

²⁰A. Abragam, *Principles of Nuclear Magnetism* (Oxford University Press, Oxford, 1961).

²¹C. P. Slichter, *Principles of Magnetic Resonance* (Springer, Berlin, 1980).

²²G. Nunes, Jr., C. Jin, A. M. Putnam, and D. M. Lee, *Phys. Rev. Lett.* **65**, 2149 (1990).

²³W. P. Kirk and M. Twerdochlib, *Rev. Sci. Instrum.* **49**, 765 (1978).

²⁴D. S. Greywall, *Phys. Rev. B* **33**, 7520 (1986).

²⁵E. D. Adams, J. M. Delrieu, and A. Landesman, *J. Phys. (Paris)* **39**, L190 (1978).

²⁶G. Nunes, Jr., *Rev. Sci. Instrum.* **61**, 1154 (1990).

²⁷W. N. Hardy and L. A. Whitehead, *Rev. Sci. Instrum.* **52**, 213 (1981).

²⁸N. Bloembergen and R. V. Pound, *Phys. Rev.* **95**, 9 (1954).

²⁹Stanley Bloom, *J. Appl. Phys.* **28**, 800 (1957).

³⁰G. Nunes, Jr., Ph.D. thesis, Cornell University, 1991.

³¹We have used the ³He effective mass $m^* = 2.255m_3$ given by A. Ghozlan and E. Varoquaux, *Ann. Phys. (Paris)* **4**, 239 (1979).

³²J. R. Owers-Bradley, R. M. Bowley, and P. C. Main, *J. Low Temp. Phys.* **60**, 243 (1985).

³³B. R. Johnson, Ph.D. thesis, Cornell University, 1984.

³⁴*Experimental Techniques in Condensed Matter Physics at Low Temperatures*, edited by R. C. Richardson and E. N. Smith (Addison-Wesley, New York, 1988).

³⁵J. C. Maxwell, *A Treatise on Electricity and Magnetism*, 3rd ed. (Oxford, London, 1892), Vol. 1, p. 434.

³⁶H. Godfrin, G. Frossati, B. Hebral, and D. Thoulouze, *J. Phys. (Paris) Colloq.* **41**, C7-275 (1980).

³⁷N. Bloembergen, *Nuclear Magnetic Relaxation* (Benjamin, New York, 1961).

³⁸W. J. Mullin, F. Laloë, and M. G. Richards, *J. Low Temp. Phys.* **80**, 1 (1990).

³⁹P. C. Hammel and R. C. Richardson, *Phys. Rev. Lett.* **52**, 1441 (1984).

⁴⁰J. F. Kelly and R. C. Richardson, in *Proceedings of the Thirteenth International Conference on Low Temperature Physics* (Plenum, New York, 1974), Vol. I, p. 167; J. F. Kelly, Ph.D. thesis, Cornell University, 1974.

⁴¹R. C. Samarungana, K. P. Martin, J. S. Brooks, and G. O. Zimmerman, *J. Appl. Phys.* **54**, 6421 (1983).

⁴²H. Godfrin, G. Frossati, D. Thoulouze, M. Chapellier, and W. G. Clark, *J. Phys. (Paris) Colloq.* **39**, C6-287 (1978).

⁴³DLX6000 is a Teflon-like polymer containing paramagnetic spins (¹⁹F) whose magnetic moment and density are not too different from the those of the protons in the sample cell epoxy. DLX6000 and Teflon are registered trademarks

- of the Dupont corporation.
- ⁴⁴R. Kumaresan and D. W. Tufts, *IEEE Trans. Acoust., Speech, Signal Process. ASSP-30*, 833 (1982); H. Barkhuijsen, R. de Beer, W. M. M. J. Bovée, and D. van Ormondt, *J. Magn. Res.* **61**, 465 (1985).
- ⁴⁵W. J. Mullin and J. W. Jeon, *J. Low Temp. Phys.* **88**, 433 (1992); W. J. Mullin (private communication).
- ⁴⁶C. Ebner, *Phys. Rev.* **156**, 222 (1967).
- ⁴⁷R. M. Bowley (private communication).
- ⁴⁸G. Deville, M. Bernier, and J. M. Delrieux, *Phys. Rev. B* **19**, 5666 (1979).
- ⁴⁹G. Eska *et al.*, *Physica B (Utrecht)* **108**, 1155 (1981).
- ⁵⁰J. S. Denker, N. P. Bigelow, D. Thompson, J. H. Freed, and D. M. Lee, *Physica B (Utrecht)* **108**, 549 (1984).
- ⁵¹R. Bowtell, R. M. Bowley, and P. Glover, *J. Magn. Res.* **88**, 643 (1990).
- ⁵²A. S. Bedford, R. M. Bowley, J. R. Owers-Bradley, and D. Wightman, *J. Low Temp. Phys.* **85**, 389 (1991).
- ⁵³J. R. Owers-Bradley, D. R. Wightman, R. M. Bowley, A. Bedford, and A. Child (unpublished); J. R. Owers-Bradley, D. R. Wightman, R. M. Bowley, and A. Bedford, *Physica B (Utrecht)* **165**, 729 (1990).
- ⁵⁴A. S. Bedford (private communication).
- ⁵⁵D. Candela (private communication).
- ⁵⁶A masing mechanism has been invoked as an explanation for the msec time-scale bursting behavior previously observed in pure ^3He (Ref. 57). That mechanism (Ref. 58) applied to our system, however, predicts an interval between bursts of only a few μsec , and a similar time scale for the overall lifetime of the signals.
- ⁵⁷F. J. Low and H. E. Rorschach, *Phys. Rev.* **120**, 1111 (1960).
- ⁵⁸J. C. Kemp, *J. Appl. Phys.* **30**, 1451 (1959).
- ⁵⁹E. M. Purcell, *Phys. Rev.* **69**, 681 (1946).
- ⁶⁰B. Castaing, *Physica B (Utrecht)* **126**, 212 (1984).
- ⁶¹A. E. Meyerovich, in *Progress in Low Temperature Physics*, edited by D. F. Brewer (North-Holland, Amsterdam, 1987), Vol. XI.
- ⁶²W. H. Press, B. P. Flannery, S. A. Teukolsky, and W. T. Vetterling, *Numerical Recipes* (Cambridge University Press, New York, 1986).
- ⁶³L. P. Lévy, *Phys. Rev. B* **31**, 7077 (1985).
- ⁶⁴See, e.g., H. C. Fogedby, *J. Phys. A* **13**, 1467 (1980).
- ⁶⁵J. R. Owers-Bradley, *Physica B (Utrecht)* **169**, 190 (1991).

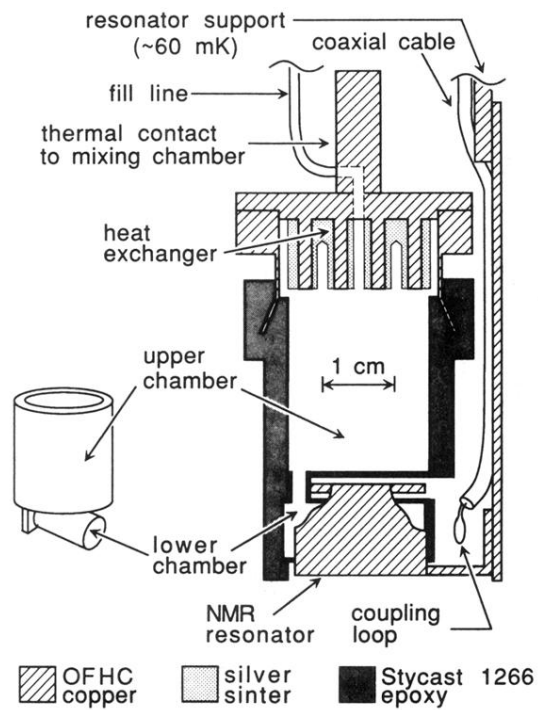


FIG. 2. Schematic view of the sample cell. The relative orientation of the upper and lower chambers is indicated by the smaller figure on the left. The NMR resonator is shown partly cut away. Note that the resonator and its support do not touch the cell.